haematologica
Journal of the Ferrata Storti Foundation

A fully humanized von Willebrand disease type 1 mouse model as unique platform to investigate novel therapeutic options

by Geneviève McCluskey, Marco Heestermans, Ivan Peyron, Eloise Pascal, Marie Clavel, Eric Bun, Emilie Bocquet, Christelle Reperant, Sophie Susen, Olivier D. Christophe, Cécile V. Denis, Peter J. Lenting and Caterina Casari

Received: June 13, 2024.
Accepted: November 21, 2024.

Citation: Geneviève McCluskey, Marco Heestermans, Ivan Peyron, Eloise Pascal, Marie Clavel, Eric Bun, Emilie Bocquet, Christelle Reperant, Sophie Susen, Olivier D. Christophe, Cécile V. Denis, Peter J. Lenting and Caterina Casari. A fully humanized von Willebrand disease type 1 mouse model as unique platform to investigate novel therapeutic options.
Haematologica. 2024 Nov 28. doi: 10.3324/haematol.2024.286076 [Epub ahead of print]

A fully humanized von Willebrand disease type 1 mouse model as unique platform to investigate novel therapeutic options

*Geneviève McCluskey[1], *Marco Heestermans[1], Ivan Peyron[1], Eloise Pascal[2], Marie Clavel[2], Eric Bun[1], Emilie Bocquet[1], Christelle Reperant[1], Sophie Susen[3], Olivier D. Christophe[1], Cécile V. Denis[1], #Peter J. Lenting[1] and #Caterina Casari[1]

[1]Université Paris-Saclay, INSERM, Hémostase inflammation thrombose HITh U1176, 94276, Le Kremlin-Bicêtre, France

[2]Inovarion, Paris, France

[3]Univ. Lille, Inserm, CHU Lille, Institut Pasteur de Lille, U1011-EGID, F-59000 Lille, France

*GM and MH contributed equally as co-first authors

#PJL and CC contributed equally as co-senior authors

Authorship Contributions: IP, MH, GMC, EP, MC, EB, CC performed experiments and analyzed data; CR performed genotyping, SS, ODC, CVD, PJL and CC conceived and supervised the study, CC wrote the first version of the manuscript. All authors contributed to data interpretation and critically reviewed & approved the final version of the study.

Running head: A VWD-type 1 humanized murine model

Correspondence: Caterina Casari, Inserm U1176, 80 rue du Général Leclerc, 94270 Le Kremlin-Bicetre, France Tel: +331-49595615; Fax: +33146719472; Email: caterina.casari@inserm.fr

Data Sharing Statement: Data are available upon reasonable request to the corresponding author

Word count abstract: 247 **Word count text**: 3863 **Figures**: 7 **Supplementary files**: 1

Acknowledgements: The authors thank Frédéric Adam for his insightful assistance with the perfusion experiments, Claire Auditeau, Delphine Borgel & Dominique Lasne for performing the VWF activity test, and Rim Hamze for technical assistance. Some figures were created using BioRender.com.

Funding: This study was funded by the French National Research Agency (Agence Nationale de la Recherche) with the Hospital-University Research in Health program (Recherche Hospitalo-Universitaire) WILL-ASSIST-HEART ANR-17-RHUS-0011 and ANR-21-CE14-0076-01.

Disclosure of Conflicts of Interest: IP, ODC, CVD, PJ and CC are co-inventors on a patent regarding KB-V13A12, patent under licence.

ABSTRACT

Patients suffering from von Willebrand disease (VWD) have reduced quality-of-life despite current treatment options. Moreover, innovation in VWD therapeutic strategies has essentially stalled and available treatments have remained unchanged for decades. Therefore, there is an unmet need to develop new therapeutic strategies for VWD-patients, especially for the large portion of those with VWD-type 1. Due to species differences, the available VWD murine models are not suitable for preclinical studies, making it difficult to test new therapeutic approaches in vivo. With this in mind, we generated mice selectively expressing human von Willebrand factor (VWF) and human GPIbα. Because this fully humanized model was found to express low VWF (12%) and FVIII (40%) levels with normal multimer profile and activity/antigen ratio, we repositioned it as a VWD-type 1 model (hVWD1 mice). In depth characterization of this model confirmed VWD-type 1 features with a decrease in platelet adhesion and thrombus formation in vitro. In vivo, a moderate bleeding phenotype was observed which was corrected upon the administration of recombinant-VWF or upon histamine-induced release of endothelial VWF. In search for new therapeutic options for VWD, we designed a bispecific single-domain antibody that bridges VWF to albumin (KB-V13A12). Remarkably, a single subcutaneous administration of KB-V13A12 coincided with a sustained 2-fold increase in VWF antigen levels for up to 10 days and normalized haemostasis in a tail-clip model in hVWD1 mice.

We have developed a unique humanized mouse model for VWD-type 1 and a promising new therapeutic that corrected haemostasis in these mice.

INTRODUCTION

Von Willebrand Disease (VWD) is the most common inherited bleeding disorder, historically categorized into three main types and further subtypes.[1] In most reported cohorts, VWD-type 1 is the most frequent type (70-80% of cases). It consists of heterogeneous quantitative deficiencies with reduced von Willebrand factor (VWF) antigen levels between 5 and 30-50% (<30, regardless of bleeding, <50 with abnormal bleeding), usually normal activity-to-antigen ratios (>0.6) and normal or minimally abnormal multimer profiles.[1–3] Unsurprisingly, such a wide range of VWF levels is associated with variable phenotypes from minor to severe bleedings, which highly contribute to the challenge of diagnosing VWD-type 1/low VWF and precisely defining cut-off levels.[4,5] Genetics and pathogenesis of VWD-type 1 are again heterogeneous. VWF levels below 30% are often associated with bleedings and hereditary dominant genetic variants, whereas *VWF* DNA alterations are less common in low VWF patients with milder levels (30-50%).[6–10] Adding to the difficulties of VWD-type 1 diagnosis are fluctuating VWF levels, which may increase with age, during pregnancy, or after exercise. Finally, some of the bleeding symptoms typical for VWD-type 1 are also found in healthy individuals, although the severity may differ.[11,12] Due to this vast heterogeneity, the molecular mechanisms responsible for VWD-type 1 have not been fully elucidated.

Diagnosis and management of patients with VWD-type 1 rely not only on laboratory results but also on the personal and familial bleeding history, which remains challenging.[13] Desmopressin, an antidiuretic that promotes VWF release from intracellular storage into the circulation, is the standard of care for these patients but has some disadvantages: 1) it remains ineffective in a small proportion of patients, 2) is difficult to manage in children, 3) is associated with tachyphylaxis, 4) can induce minor side effects in some patients and 5) is only produced by one company, which causes supply issues.[14]

In the context of haemostasis, mouse models are irreplaceable tools to untangle the pathophysiology of disorders and to develop new therapeutic strategies. One of the major limitations of studying VWF in murine models is the human/mouse incompatibility between VWF and the platelet receptor GPIbα. In contrast to murine-(m)VWF, which can bind to human-(h)GPIbα in vivo, although with a reduced affinity,[15–17] human-VWF binds poorly to the murine receptor, preventing the normal recruitment of platelets at sites of injury. To overcome this limitation, several chimeric approaches have been developed.[17–19] The present study, describes the first fully humanized murine model expressing full-length hVWF and hGPIbα. Because this model was found to recapitulate the characteristics of VWD-type 1, they will be referred to as hVWD1 mice throughout the manuscript. hVWD1 mice have a mild bleeding phenotype that can be rapidly but shortly normalized by exogenous administration of recombinant hVWF concentrate or by the release of

intracellular pools of VWF. Sustained haemostatic improvement was also observed with a bispecific single-domain antibody (sdAb) designed to increase VWF levels. Altogether, these engineered mice represent a new and exclusive platform for studying VWD-type 1 and appear to be a promising tool for developing & testing innovative therapeutic approaches for VWD.

METHODS

A detailed description of the experimental procedures can be found in the Supplementary online information.

Animal and ethic statement

This project (number APAFIS #32699-2021081611421076 v1) was approved by the local ethical committee of Université Paris-Sud (comité d'éthique en expérimentation animale no. 26).

Engineering of hVWD1 mice

Transgenic mice expressing hVWF and hGPIbα instead of the corresponding murine proteins (Figures 1A-B, respectively) were engineered in a pure 129S2 genetic background known to express functional ADAMTS13 (a disintegrin and metalloproteinase with a thrombospondin type 1 motif, member 13)[20,21] (genOway, Lyon, France). 129S2Crl-*Vwf*$^{-/-}$-Tg(*VWF)* mice and 129S2Crl-*Gp1ba*$^{-/-}$-Tg*(GP1BA)* mice, were intercrossed to generate double knock-in mice 129S2Crl-*Vwf*$^{-/-}$-Tg(*VWF),Gp1ba*$^{-/-}$-Tg*(GP1BA),* which will be referred to as hVWD1. Littermate controls will be referred as 129S2 (Figure 1C).

PCR products for genotyping were separated by electrophoresis (Figure 1D).

VWF-FVIII assays

VWF antigen (VWF:Ag) levels[22] and multimer profiles[23,24] were assessed as previously described. VWF activity was measured with a collagen binding (VWF:CB) and a platelet-dependent assay (VWF:GPIbR).

FVIII activity (FVIII:C) was measured using the chromogenic Biophen FVIII-assay kit (Hyphen, Neuville-sur-Oise, France) as instructed.

Parallel plate flow perfusion

Thrombus formation was evaluated using a Maastricht flow chamber in a whole-blood perfusion assay on a fibrillar collagen matrix under arterial shear conditions (shear rate of 3000 s^{-1}). Single dots in the graph represent individual mice (average value of 20 images).

KB-V13A12 production and administration

SdAbs against VWF were generated[25] and sdAb KB-V13 (formerly KB-VWF-013) binding h/mVWF has been previously characterized.[26] KB-V13 recognizes the D'D3 region of VWF and does not interfere with the FVIII binding to VWF. The anti-albumin KB-OptiAlb12 is a llama-derived sdAb that displays high-affinity binding (<5 nM) to both human and murine albumin. KB-V13A12, combining the two sdAbs, was expressed in competent E.coli WK6 bacteria and purified by affinity chromatography. A control bispecific sdAb (KB-V13AT02) was synthetized by cloning the KB-V13 linked to the previously described KB-AT02 against antithrombin.[27]

Purified bispecific sdAbs were administered subcutaneously (SC) (5mg/kg body weight).

Tail vein transection model and tail artery transection model

Tail-vein-transection (TVT) was conducted as described.[28]

The tail artery transection (TAT) model consisted of a modified TVT in which the ventral tail artery was transected using the same customized templates. Experimental time was set at 30 minutes.

Tail-clip model

A tail-clip assay was performed as described.[29,30]

Histamine (Merck, Fontenay Sous Bois, France) was administered intraperitoneally (13µmol/kg body weight)[31] 30 minutes prior to the procedures.

Recombinant hVWF (r-hVWF, Veyvondi, Takeda) was administered IV (50U/Kg body weight) 5 minutes before the procedures.

Saphenous vein puncture model

The saphenous vein puncture model was conducted as described.[32]

Thrombosis model

In vivo thrombus formation in the carotid artery was induced by 15% ferric-chloride.

Statistical analysis

All data are presented as mean±standard deviation (mean±SD). Numbers (n) refer to individual animals. The statistical analysis was performed using GraphPad Prism 10 software (La Jolla,

California, USA). One-way analysis of variance (1-way ANOVA) followed by Tukey's or Dunnett's multiple comparison test was performed when comparing multiple groups. Pairwise analysis was performed using the unpaired two-tailed Student's t-test, unless otherwise stated. Two-way analysis was performed for two factors comparisons. $P<0.05$ was considered as statistically significant.

RESULTS

hVWD1 mice are viable and fertile

By using the targeting strategy outlined in Figure 1, hVWD1 mice expressing hVWF (wild-type) and hGPIbα (wild-type), were generated. Intercross of heterozygous mice for each transgene to obtain homozygous mice 129S2Crl-*Vwf*$^{-/-}$-Tg(*VWF)* named hVWF mice and 129S2Crl-*Gp1ba*$^{-/-}$-Tg*(GP1BA)* named hGP1BA mice, resulted in mendelian distribution of genotypes (not shown), suggesting that expression of the human version of VWF and GPIbα proteins in mice does not impair murine embryonic development or perinatal survival. Homozygous hVWF and hGP1BA mice were then intercrossed to obtain homozygous, double humanized mice named hVWD1 (129S2Crl-*Vwf*$^{-/-}$-Tg(VWF), *Gp1ba*$^{-/-}$-Tg(GP1BA), Figure 1C).

hVWD1 mice express human VWF and have a normal multimer profile

Because hVWD1 mice express hVWF and littermate controls express mVWF, VWF:Ag levels cannot be compared in the two groups of mice. Therefore, VWF:Ag levels for hVWD1 mice were quantified using human pooled normal plasma (hPNP) as reference, finding that average VWF:Ag levels were 12±3% (n=51; Figure 2A). VWF activity was measured with a VWF:CB and a VWF:GPIbR assays. Activity/antigen ratios were similar for the two assays (0.8±0.2, n=7, Figure 2B). FVIII:C levels were also reduced compared to control mice (40±9% and 117±17%, respectively, $p<0.001$, Figure 2C). Both, VWF:Ag and FVIII:C levels were relatively stable over a 15/17-week time period (Figure S1A-B).

Despite the quantitative defect, multimer profiles of plasmatic VWF showed normal distribution of low, medium and high molecular weight multimers (HMWMs), consistent with VWD-type 1 profiles in patients (Figure 2D, lanes 1-2). Multimers were characterized by the typical triplets that are also observed in human plasma, suggesting that hVWF expressed in mice is cleaved by mADAMTS13 in a similar way as in humans (Figure 2D, lanes 3-4).

The presence of hVWF was validated in an immunosorbent assay using monoclonal antibodies selectively recognizing hVWF (Figure S2). Although in an indirect manner, these analyses also supported the absence of mVWF in hVWD1 mice. Exclusive human or murine GPIbα expression on platelets was validated by flow cytometry using species-specific monoclonal antibodies (Figure S3) and by immunofluorescence on blood smears (not shown).

Mice expressing hGPIbα have been previously generated with a similar genetic approach and their platelets & GPIb-IX-V complex characterized[15,16]. We tested platelet counts, volume and activation (Figure S4). Peripheral platelet count was modestly decreased in hVWD1 compared to control mice (471±47 and 592±65*10^3/µl, respectively, P<0.001, Figure S4A), while platelet size was moderately increased (6±0.3 and 5±0.3µm^3, Figure S4B). Despite these minor differences, agonist-induced platelet activation was similar between the two groups (Figure S4C-D).

We also assessed VWF in platelets and found that hVWD1 mice have a minor reduction in platelet-VWF content, compared to human platelets or 129S2-platelets (Figure S5). Importantly, platelet-VWF was slightly enriched in HMWMs, akin to VWF in human platelets (Figure S5).

VWF function was evaluated using classic parallel plate perfusion chambers at elevated shear rate (3000s^{-1}), at which platelet tethering is highly dependent on VWF.[33,34] Consistent with low VWF:Ag in circulation and minor platelet-VWF reduction, only some small thrombi were formed in hVWD1-mice (Figure 2E). Platelet-covered surface and fluorescence intensity were 4-6-fold decreased compared to control-mice (% of covered-surface 5.2±1.9 *versus* 19.6±3.4, fluorescence a.u. 241±126.2 *versus* 1367±480.2, respectively; P<0.001, Figure 2F-G), suggesting that the reduced VWF levels are insufficient to support normal thrombus formation in hVWD1 mice.

hVWD1 mice have a mild bleeding phenotype and a modestly reduced response to ferric chloride

To thoroughly characterize this model of VWD-type 1, haemostasis and thrombosis were assessed using in vivo assays of various severity.

First, the difference between the amount of blood shed by hVWD1 and control mice was not statistically significant (84±82 and 36±22µl, respectively, P=0.1223, Figure 3A) when assessed in the TVT model. In addition, bleeding profiles were similar between both groups (Figure 3B), showing that hVWD1 mice exhibited similar haemostasis as control mice in this particular model.

We next applied more severe models. In a TAT assay, the bleeding tendency of hVWD1 mice was higher than that of control mice, with 2-fold more of blood shed from the injury (511±232 and 245±184µl, respectively, P=0.0082, Figure 3C) and longer bleeding times in hVWD1 mice (Figure 3D). In a tail-clip assay, despite some variability, the amount of blood shed over 30 minutes was increased 5-fold in hVWD1- compared to control-mice (102±122 and 18±37µl, respectively, P=0.0004, Figure 3E) and the time of the first bleeding arrest was substantially delayed (463±s624 in hVWD1 mice and 88±s49 in control mice, P=0.0095, Figure 3F). Finally, in a model of large saphenous vein puncture, the number of clots formed during the 30-minute observation time, was notably decreased in hVWD1 versus control mice (12±5 versus 20±4 clots, respectively, P<0.0001,

Figure 3G), which also coincided with relatively longer bleeding times (not shown). Overall, these data indicate that hVWD1 mice display a moderate bleeding phenotype recapitulating the profile of a large part of patients with this disease.

In addition, we evaluated $FeCl_3$-induced thrombus formation in the carotid artery of hVWD1- and control-mice. hVWD1 had reduced response to $FeCl_3$ (Figure 4). The decrease in blood flow upon $FeCl_3$ administration, a proxy for progressive vessel occlusion, was slower and less pronounced in hVWD1- than in control mice, resulting in a higher area under the curve (697±267 versus 393±121a.u., respectively P=0.0260, Figure 4A-B). Occlusion was delayed in hVWD1 mice but failed to reach statistically significant difference between both groups (14±8.1 versus 8.1±2.2s, respectively P=0.0649; one out of 6 hVWD1 did not occlude, Figure 4C).

Recombinant human VWF is functional and restores haemostasis in hVWD1 mice

We evaluated whether restoring VWF normal levels using r-hVWF would be functional in our hVWD1 mice. Mice were administered with 50U/kg of r-hVWF (therapeutic dose) and VWF antigen, multimers and haemostasis were assessed 5 minutes post IV injection. VWF:Ag levels increased ≈6-fold post-infusion, reaching 76±5.2% (Figure 5A). As expected, when evaluated in medium-resolution gels, multimer profiles were similar before- and post-r-hVWF administration, however, due to higher protein concentration, bands corresponding to multimers of almost all molecular weight appeared more sharp post-infusion (Figure 5B-C). Densitometry suggested that r-hVWF administration resulted in an enrichment of medium-MWMs (Figure 5C). A separate group of mice were subjected to a tail-clip assay (Figure 5D). The amount of blood shed by hVWD1 mice receiving r-hVWF (64±82 µl, magenta) was similar to that shed by control mice (19±37µl, yellow, P=0.5290) and coincided with normalization of the bleeding time (not shown). These data demonstrate that r-hVWF is functional and restores haemostasis in hVWD1 mice.

Agonist-induced release of endothelial hVWF restores haemostasis in hVWD1 mice

To explore whether intracellular VWF could be released in circulation and affect haemostasis, we triggered histamine-induced endothelial degranulation (as a surrogate for desmopressin).[31] Thirty minutes after intraperitoneal administration of histamine to hVWD1 mice, circulating VWF:Ag was significantly increased in 14 out of 15 mice (from 13±3% to 17±2%; p<0.0001; Figure 6A). Because VWF stored in Weibel-Palade bodies is known to be enriched in HMWMs, we also performed multimer analysis. To minimize inter-gel differences, plasmas collected from the same mouse, before and after histamine administration were loaded in consecutive lanes, after normalization of VWF concentrations (Figure 6B). Densitometric analysis showed that multimer profiles were shifted

toward increased levels of HMWMs post- (black profiles) compared to pre-injection (grey, Figure 6C), in the majority of mice (8 out of 11). Despite the variable antigen response, the quantitative increase, paired with the multimer improvement, was sufficient to sustain haemostasis in the tail-clip model (19±37µl yellow-control mice and 48±62µl blue-hVWD1 mice receiving histamine, P=0.6928, Figure 6D). These data indicate that, similar to humans, hVWD1 mice have a pool of highly multimerized, functional VWF, which can be rapidly released in circulation.

hVWD1 mice are instrumental in developing new therapeutic molecules: the example of KB-V13A12

Despite currently available treatments for patients with VWD-type 1 being considered quite effective, recurrent bleedings are still reported, especially in patients with the potential to menstruate suffering from menorrhagia.

In search for novel therapeutic options, we generated a bispecific antibody composed of a non-inhibitory anti-VWF(D'D3) sdAb[26] linked to a sdAb recognizing human and murine albumin, named KB-V13A12.[35] While thorough characterization of this bispecific sdAb will be discussed in a separate study (in preparation), the hVWD1 mice seemed to be the perfect platform to test this molecule. Following its administration (5mg/kg), VWF levels were determined over a 14-day period, while the tail-clip procedure was performed three days after administration, in another series of mice. The 5mg/kg dose was selected based on a dose-effect curve (Figure S6). Remarkably, VWF antigen levels rapidly increased one-day post-injection, achieving a relatively stable near 2-fold increase between 3- and 10-days post-injection (11±2% pre- versus 21±3% 3-day post- and 19±3% 10-day post-administration, P<0.0001, Figure 7A, green). As a control, the administration of a bispecific sdAb targeting VWF and antithrombin (KB-V13AT02) had no effects on VWF levels (Figure 7A, grey).

We also tested two conditions for multimer analysis. First, total amount of VWF was normalized (Figure 7B, samples M9-M10) at the expense of having to use different ratios of plasma and buffer between pre- and post-administration samples. In these conditions, we observed that the overall multimer profile remained unaffected by administration of KB-V13A12 (Figure 7C). Triplets were visible only in post-administration samples having the lower plasma/buffer ratio. Consistent with normal triplet structure, the central band was more intense compared to satellite bands, suggesting that VWF degradation was not perturbed. In the second condition, we loaded the maximum amount of VWF for each sample, keeping the plasma/buffer ratio identical between pre- and post-treatment samples (Figure 7B-C, samples M11-M12). In these conditions, multimers of all molecular weight appeared increased post-KB-V13A12 infusion, suggesting that the sdAb is able to bind multimers of any molecular size.

Finally, tail-clip was performed 3 days post-treatment (Figure 7D). One single SC administration of KB-V13A12 was sufficient to restore haemostasis of hVWD1 mice by normalizing the amount of blood shed upon injury in a quite severe bleeding model (19±37µl in control- (yellow) and 47±49µl in hVWD1 mice receiving KB-V13A12 (green), P=0.7111).

DISCUSSION

VWD-type 1 is the most frequent VWD-type but also one of the most heterogeneous, making it difficult to diagnose and manage, especially in patients with mild VWF levels, also referred to as low VWF.[4,12] Despite the high prevalence of this VWD-type, the only available murine model, so far, is the RIIIS/J mouse expressing low levels of mVWF, FVIII and factor XI.[36,37] These mice have been instrumental to link aberrant post-translational modifications to elevated VWF clearance, however, their use as models to test therapeutic molecules is limited. In the present study, we report on the fortuitous creation and characterization of the first fully humanized VWD-type 1 model (hVWD1 mice) and its unique use as a platform to test new therapeutic strategies, one of which is presented here.

Patients with VWD-type 1 and VWF levels below 30% often carry dominant genetic variants within the *VWF* gene. The hVWD1 mice express low levels (≈12%) of normal hVWF without any pathological genetic variant within the *VWF* gene. Several mechanisms associated with genomic engineering could contribute to these low levels and are not mutually exclusive: a) the absence of intronic regulatory sequences, missing because only the h-cDNA has been inserted in the m-genome, b) expression of the hVWF under the control of endogenous murine regulatory elements, which have not been humanized and c) structural differences due to genomic rearrangements somehow affecting transcription of the h-cDNA and protein expression.

One major functional complication needs to be carefully considered when expressing hVWF in murine models. VWF accomplishes its functions by binding to its partners and, during primary haemostasis, it is essential to initiate tethering of platelets to the sub-endothelium at sites of vascular injury. However, due to a human/mouse incompatibility between VWF and GPIbα, hVWF poorly interacts with murine platelets. In the past, to overcome this limitation, our group and others have engineered one partner or the other by creating chimeric models able to sustain VWF/platelet interaction.[17–19] To the best of our knowledge, the hVWD1 mice are the first model expressing fully humanized VWF and GPIbα.

Consistent with previous data,[16,17,38] expression of hGPIbα in mice is associated with slightly perturbed platelet count and size but had no functional haemostatic effects (Figure S4).

Accurate analysis of multimer profiles is an essential step for VWF studies, however, it remains technically challenging and protocols vary from one laboratory to another. Because hVWD1 mice express hVWF in murine plasma, no perfect reference is available, therefore we studied VWF multimers in different conditions. Using standard sample dilutions, we confirmed that multimers of all sizes circulate in hVWD1 murine plasma as in human plasma (Figure 2D). Some mouse strains, including the C57Bl/6J, express a less functional ADAMTS13, which is missing the carboxy-terminal thrombospondin type 1 repeat and CUB domains.[21] To overcome this limitation, we generated the hVWD1 mice in a 129S2 genetic background and visualized similar triplet structures in hVWD1 mice as in human plasma (Figure 2D, lanes 3-4).

Patients with VWD-type 1 often experience mucocutaneous bleedings such as bruising, epistaxis, oral bleeds, bleeds from minor wounds and menorrhagia.[4] To evaluate the bleeding tendency of the transgenic mice, we assessed haemostasis in assays of different severity (Figure 3). In the TVT model, the hVWD1 mice have a rather normal response, similar to control mice. In three more severe models, however, hVWD1 mice display a mild-to-moderate bleeding tendency, consistent with a large proportion of patients' phenotypes. We also observed in hVWD1 mice, as in patients, that bleeding phenotype is quite variable. This suggests that ~12% VWF:Ag levels, likely reflect the threshold amount of VWF necessary to maintain haemostasis in mice and small variations (7.3-18%, minimum-maximum VWF:Ag range) are sufficient to shift the balance towards bleeding or not. Moreover, other than from plasma, VWF from other physiologic compartments (i.e. endothelial cells and platelets) is present in hVWD1 mice and likely contribute to the hemostatic response. In hVWD1 mice, endothelial-VWF mobilization and contribution was demonstrated by the correction of the bleeding tendency upon histamine administration (Figure 6), a proxy for desmopressin, the first treatment option for VWD-type 1 patients. For those not responding to desmopressin, VWF concentrates are the best option. Similar to patients, therapeutic doses of r-hVWF corrected the bleeding tendency of hVWD1 mice (Figure 5). Abnormal haemostatic behavior in hVWD1 mice was further confirmed by reduced thrombus formation over collagen surfaces in perfusion assays (Figure 2E-F-G) and by a delayed response to ferric chloride in vivo (Figure 4), which are most likely due to the VWF-defect[39] rather than hGPIbα expression.[17,40] Altogether, these experiments validate the hVWD1 transgenic mice as models of VWD-type 1.

In search for innovative therapeutic options that could be safe, efficient and long-acting, we developed a bispecific sdAb[41] (KB-V13A12) that simultaneously binds albumin and VWF. We hypothesized that VWF bridged to albumin by the nanobody should follow albumin in the FcRn-mediated recycling pathway within the endothelial cells[42] and that this mechanism should increase circulating VWF levels. In vivo, one subcutaneous administration of KB-V13A12 to hVWD1 mice was

associated with a sustained 2-fold increase in VWF:Ag levels for up to 10 days and an increase of multimers of all molecular weights (Figure 7A-B-C). Furthermore, KB-V13A12 was as efficient as r-hVWF and histamine in correcting haemostasis (Figure 7D). Based on this data, we believe that KB-V13A12 has the potential to be a new treatment option for VWD, particularly VWD-type 1.

It is important to emphasize that heterogenous bleeding symptoms may manifest in VWD, including gender-specific bleeding in people with the potential to menstruate, who still experience increased depression, anxiety, and low quality-of-life.[43–46] Because of its effects on circulating VWF levels, we believe that KB-V13A12 should be further investigated in the context of various bleeding symptoms.

Currently, several murine models for severe VWD subtypes are available and have been crucial for our understanding of the pathophysiology of VWD.[39,47–50] Here, we report the first humanized murine model for the most common mild/moderate forms of VWD. Besides their help in dissecting molecular pathways, humanized models are very useful for translational research, for testing therapeutic, diagnostic molecules that directly bind their target (i.e, antibodies such as the KB-V13A12). Apart from hVWD1 mice, other variants (type 2A, type 2M or type 2N) could also be developed for this purpose.

Some limitations should be considered when using hVWD1 mice. These mice have a 129Sv genetic background, which complexifies and increases the costs of breeding and colony management. Most in vivo assays have been originally developed in C57Bl/6 mice and should be internally validated for the 129 mice. The hVWD1 mice expressing ~12% of hVWF exhibit a certain degree of variability in the in vivo assays. Therefore, the choice of the specific assay and the number of animals is key in every experiment. Because of the humanization of VWF and GPIbα, the best reference/control condition should be carefully considered for each experiment. As for some VWD-type 1 patients, the molecular mechanism explaining the low VWF levels in the hVWD1 mice is still unclear, which can limit some interpretation and exploitation.

Our study indicates that, despite some limitations, this humanized model is a unique platform for preclinical testing of innovative therapeutic options overcoming the species/species incompatibility between hVWF and mGPIba.

REFERENCES

1. Leebeek FWG, Eikenboom JCJ. Von Willebrand's Disease. N Engl J Med. 2016;375(21):2067-2080.

2. James PD, Connell NT, Ameer B, et al. ASH ISTH NHF WFH 2021 guidelines on the diagnosis of von Willebrand disease. Blood Adv. 2021;5(1):280-300.

3. Sadler JE, Budde U, Eikenboom JC, et al. Update on the pathophysiology and classification of von Willebrand disease: a report of the Subcommittee on von Willebrand Factor. J Thromb Haemost. 2006;4(10):2103-2114.

4. Bowman ML, James PD. Controversies in the diagnosis of Type 1 von Willebrand disease. Int J Lab Hematol. 2017;39(Suppl 1):61-68.

5. Sadler JE. Low von Willebrand factor: sometimes a risk factor and sometimes a disease. Hematology Am Soc Hematol Educ Program. 2009;106-112.

6. Cumming A, Grundy P, Keeney S, et al. An investigation of the von Willebrand factor genotype in UK patients diagnosed to have type 1 von Willebrand disease. Thromb Haemost. 2006;96(5):630-641.

7. Goodeve A, Eikenboom J, Castaman G, et al. Phenotype and genotype of a cohort of families historically diagnosed with type 1 von Willebrand disease in the European study, Molecular and Clinical Markers for the Diagnosis and Management of Type 1 von Willebrand Disease (MCMDM-1VWD). Blood. 2007;109(1):112-121.

8. Flood VH, Christopherson PA, Gill JC, et al. Clinical and laboratory variability in a cohort of patients diagnosed with type 1 VWD in the United States. Blood. 2016;127(20):2481-2488.

9. James PD, Notley C, Hegadorn C, et al. The mutational spectrum of type 1 von Willebrand disease: Results from a Canadian cohort study. Blood. 2007;109(1):145-154.

10. James P, Leebeek F, Casari C, Lillicrap D. Diagnosis and treatment of von Willebrand disease in 2024 and beyond. Haemophilia. 2024;30(Suppl 3):103-111.

11. Sidonio RF, Lavin M. Diagnostic pitfalls and conundrums in type 1 von Willebrand disease. Hematology Am Soc Hematol Educ Program. 2022;2022(1):618-623.

12. Sadler JE. Von Willebrand disease type 1: a diagnosis in search of a disease. Blood. 2003;101(6):2089-2093.

13. Abou-Ismail MY, James PD, Flood VH, Connell NT. Beyond the guidelines: how we approach challenging scenarios in the diagnosis and management of von Willebrand disease. J Thromb Haemost. 2023;21(2):204-214.

14. Denis CV, Susen S, Lenting PJ. von Willebrand disease: what does the future hold? Blood. 2021;137(17):2299-2306.

15. Ware J, Russell SR, Marchese P, Ruggeri ZM. Expression of human platelet glycoprotein Ib alpha in transgenic mice. J Biol Chem. 1993;268(11):8376-8382.

16. Ware J, Russell S, Ruggeri ZM. Generation and rescue of a murine model of platelet dysfunction: the Bernard-Soulier syndrome. Proc Natl Acad Sci U S A. 2000;97(6):2803-2808.

17. Kanaji S, Orje JN, Kanaji T, et al. Humanized GPIbα–von Willebrand factor interaction in the mouse. Blood Adv. 2018;2(19):2522-2532.

18. Navarrete AM, Casari C, Legendre P, et al. A murine model to characterize the antithrombotic effect of molecules targeting human von Willebrand factor. Blood. 2012;120(13):2723-2732.

19. Chen J, Tan K, Zhou H, Lo H-F, et al. Modifying murine von Willebrand factor A1 domain for in vivo assessment of human platelet therapies. Nat Biotechnol. 2008;26(1):114-119.

20. Banno F, Kaminaka K, Soejima K, Kokame K, Miyata T. Identification of Strain-specific Variants of Mouse Adamts13 Gene Encoding von Willebrand Factor-cleaving Protease. J Biol Chem. 2004;279(29):30896-30903.

21. Zhou W, Bouhassira EE, Tsai H-M. An IAP retrotransposon in the mouse ADAMTS13 gene creates ADAMTS13 variant proteins that are less effective in cleaving von Willebrand factor multimers. Blood. 2007;110(3):886-893.

22. Lenting PJ, Westein E, Terraube V, et al. An experimental model to study the in vivo survival of von Willebrand factor. Basic aspects and application to the R1205H mutation. J Biol Chem. 2004;279(13):12102-12109.

23. Pruthi RK, Daniels TM, Heit JA, Chen D, Owen WG, Nichols WL. Plasma von Willebrand factor multimer quantitative analysis by in-gel immunostaining and infrared fluorescent imaging. Thromb Res. 2010;126(6):543-549.

24. Groot E, Fijnheer R, Sebastian SA, de Groot PG, Lenting PJ. The active conformation of von Willebrand factor in patients with thrombotic thrombocytopenic purpura in remission. J Thromb Haemost. 2009;7(6):962-969.

25. Aymé G, Adam F, Legendre P, et al. A Novel Single-Domain Antibody Against von Willebrand Factor A1 Domain Resolves Leukocyte Recruitment and Vascular Leakage During Inflammation-Brief Report. Arterioscler Thromb Vasc Biol. 2017;37(9):1736-1740.

26. Muczynski V, Casari C, Moreau F, et al. A factor VIII-nanobody fusion protein forming an ultrastable complex with VWF: effect on clearance and antibody formation. Blood. 2018;132(11):1193-1197.

27. Barbon E, Ayme G, Mohamadi A, et al. Single-domain antibodies targeting antithrombin reduce bleeding in hemophilic mice with or without inhibitors. EMBO Mol Med. 2020;12(4):e11298.

28. Johansen PB, Tranholm M, Haaning J, Knudsen T. Development of a tail vein transection bleeding model in fully anaesthetized haemophilia A mice - characterization of two novel FVIII molecules. Haemophilia. 2016;22(4):625-631.

29. Rayes J, Hollestelle MJ, Legendre P, et al. Mutation and ADAMTS13-dependent modulation of disease severity in a mouse model for von Willebrand disease type 2B. Blood. 2010;115(23):4870-4877.

30. Marx I, Lenting PJ, Adler T, Pendu R, Christophe OD, Denis CV. Correction of bleeding symptoms in von Willebrand factor-deficient mice by liver-expressed von Willebrand factor mutants. Arterioscler Thromb Vasc Biol. 2008;28(3):419-424.

31. Zirka G, Robert P, Tilburg J, et al. Impaired adhesion of neutrophils expressing Slc44a2/HNA-3b to VWF protects against NETosis under venous shear rates. Blood. 2021;137(16):2256-2266.

32. Buyue Y, Whinna HC, Sheehan JP. The heparin-binding exosite of factor IXa is a critical regulator of plasma thrombin generation and venous thrombosis. Blood. 2008;112(8):3234-3241.

33. Ruggeri ZM. The role of von Willebrand factor in thrombus formation. Thromb Res. 2007;120(Suppl 1):S5-S9.

34. Pugh N, Simpson AMC, Smethurst PA, de Groot PG, Raynal N, Farndale RW. Synergism between platelet collagen receptors defined using receptor-specific collagen-mimetic peptide substrata in flowing blood. Blood. 2010;115(24):5069-5079.

35. Peyron I, Casari C, Christophe OD, Lenting PJ DC. KB-V13A12, a novel nanobody-based therapeutic molecular for the treatment of von Willebrand disease. Int Soc Thromb Haemost. 2023;Online abs(OC):8.3.

36. Sweeney JD, Novak EK, Reddington M, Takeuchi KH, Swank RT. The RIIIS/J inbred mouse strain as a model for von Willebrand disease. Blood. 1990;76(11):2258-2265.

37. Mohlke KL, Purkayastha AA, Westrick RJ, et al. Mvwf, a dominant modifier of murine von Willebrand factor, results from altered lineage-specific expression of a glycosyltransferase. Cell. 1999;96(1):111-120.

38. Kanaji T, Russell S, Ware J. Amelioration of the macrothrombocytopenia associated with the murine Bernard-Soulier syndrome. Blood. 2002;100(6):2102-2107.

39. Denis C, Methia N, Frenette PS, et al. A mouse model of severe von Willebrand disease: defects in hemostasis and thrombosis. Proc Natl Acad Sci U S A. 1998;95(16):9524-9529.

40. Guerrero JA, Shafirstein G, Russell S, et al. In vivo relevance for platelet glycoprotein Ibα residue Tyr276 in thrombus formation. J Thromb Haemost. 2008;6(4):684-691.

41. Peyron I, Kizlik-Masson C, Dubois MD, et al. Camelid-derived single-chain antibodies in hemostasis: Mechanistic, diagnostic, and therapeutic applications. Res Pract Thromb Haemost. 2020;4(7):1087-1110.

42. Chaudhury C, Mehnaz S, Robinson JM, et al. The major histocompatibility complex-related Fc receptor for IgG (FcRn) binds albumin and prolongs its lifespan. J Exp Med. 2003;197(3):315-322.

43. Lavin M, Aguila S, Dalton N, et al. Significant gynecological bleeding in women with low von Willebrand factor levels. Blood Adv. 2018;2(14):1784-1791.

44. Roberts JC, Kulkarni R, Kouides PA, et al. Depression and anxiety in persons with Von Willebrand disease. Haemophilia. 2023;29(2):545-554.

45. Lenting PJ, Kizlik-Manson C, Casari C. Towards novel treatment options in von Willebrand disease. Haemophilia. 2022;28(S4):5-10.

46. Casari C, Leung J, James PD. New and Emerging Therapies for Women, Girls and People with the Potential to Menstruate with VWD. Blood Adv. 2023;7(24):7501-7505.

47. Adam F, Casari C, Prévost N, et al. A genetically-engineered von Willebrand disease type 2B mouse model displays defects in hemostasis and inflammation. Sci Rep. 2016;6:26306.

48. Shi Q, Fahs SA, Mattson JG, et al. A novel mouse model of type 2N VWD was developed by CRISPR/Cas9 gene editing and recapitulates human type 2N VWD. Blood Adv. 2022;6(9):2778-2790.

49. Kanaji S, Morodomi Y, Weiler H, et al. The impact of aberrant von Willebrand factor-GPIbα interaction on megakaryopoiesis and platelets in humanized type 2B von Willebrand disease model mouse. Haematologica. 2022;107(9):2133-2143.

50. Slobodianuk TL, Kochelek C, Foeckler J, Kalloway S, Weiler H, Flood VH. Defective collagen binding and increased bleeding in a murine model of von Willebrand disease affecting collagen IV binding. J Thromb Haemost. 2019;17(1):63-71.

FIGURE LEGENDS

Figure 1. Engineering of hVWD1 mice.

Panel A. Targeting vector comprising the whole coding sequence (cds) of *human VWF* followed by a hGH (human growth hormone) polyadenylation site (polyA). A neomycin positive selection cassette (Neo) flanked by two loxP sites was inserted downstream of the polyA site and a Diphteria toxin negative selection cassette (DTA) was inserted outside the homologous recombination area, upstream of exon 5. Following homologous recombination and double selection of embryonic stem cells, the recombined locus bore the *hVWF* cds followed by a Neo cassette flanked by two loxP sites. After injection of ES cells into blastocysts and breeding of the generated mice with 129Sv Cre-deleter mice, the Neo cassette was excised and heterozygous mice carrying the mutant allele were generated. Heterozygous mice were intercrossed to generate homozygous mice 129S2Crl-*Vwf*$^{-/-}$-Tg(*VWF)* mice named hVWF. **Panel B.** Targeting vector comprising the whole cds of *human GP1BA*. A Neo positive selection cassette flanked by two FRT sites was inserted downstream of the polyA site and a DTA negative selection cassette was inserted outside the homologous recombination area, upstream of exon 1. Following homologous recombination and double selection of embryonic stem cells, the recombined locus bore the *hGP1BA* cds followed by a Neo cassette flanked by two FRT sites. After injection of ES cells into blastocysts and breeding of the generated mice with 129Sv FLP-deleter mice, the Neo cassette was excised and heterozygous mice carrying the mutant allele were generated. Heterozygous mice were intercrossed to generate homozygous 129S2Crl-*Gp1ba*$^{-/-}$-Tg*(GP1BA)* mice named hGP1BA. **Panel C.** Schematic of the breeding strategy. Homozygous hVWF and hGP1BA were crossed to generate double-transgenic mice, referred as hVWD1 and control mice, referred as 129S2 mice. **Panel D.** Representative PCR products in transgenic mice expressing human or murine *VWF* and *GPIba*. Primers, P1, P2, P3, P4 and P5 as indicated in A and B. Primer sequences are reported in Supplemental table 1.

Figure 2. VWF and FVIII in hVWD1 mice.

Panel A. VWF antigen (VWF:Ag) levels in hVWD1 mice compared to a human pooled normal plasma (n=51). **Panel B.** VWF activity/antigen ratio for hVWD1 mice (n=7). VWF activity was assessed in a VWF:CB and a VWF:GPIbR assays. (Normal ratios >0.7). **Panel C.** FVIII activity (FVIII:C) levels in hVWD1 (n=42, purple) and control (n=10, yellow) mice compared to a murine pooled normal plasma. **Panel D, left.** Representative plasmatic VWF multimer profiles in 2% agarose gels. Colorimetric detection. Lanes 1 and 2 were prepared with standard sample dilution and similar amount of total VWF loaded (≈25ng). Lanes 3 and 4, were prepared to minimize the amount of murine plasma loaded in each sample. Total amount of VWF was ≈15ng. The dotted line indicates

non-adjacent lanes on the same gel. Lanes 3 and 4 were loaded on a different gel. **Panel D, middle.** Densitometric analysis of multimers in D. **Panel D, right.** Triplet structures are shown at higher magnification for some of the profiles (blue boxes). **Panel E.** Representative images of thrombi formed during perfusion of blood collected from hVWD1- (upper) and control -mice (bottom) over a collagen-coated surface at $3000s^{-1}$. Pictures were randomly selected over a total of 160-200 acquired images (20 images/perfusion, every perfusion was performed with blood collected from individual mice). **Panels F-G.** Quantification of the percentage of surface covered by platelets (F) and mean fluorescence intensity (G) in hVWD1 mice (n=8, purple) versus control mice (n=10, yellow).

A-B-C-F-G. Grey bars indicate mean±SD. Statistical analysis: C-F-G Unpaired two-tailed Student's t-test.

a.u. arbitrary units, *low* indicates VWF-LowMWMs and *high* indicates HighMWMs.

Figure 3. Haemostasis is mildly altered in hVWD1 mice

Panel A. Schematic representation of a tail-vein-transection (TVT) assay indicating the injured vessel. Amount of blood shed by hVWD1 (n=14, purple) and control (n=10, yellow) mice during the 60-minute experimental time. **Panel B.** Representative bleeding profiles in the two groups of mice. Filled bars indicate active bleedings, empty bars indicate non-bleeding periods. Dotted lines at 15-30 and 45-minute indicate clot removal (challenge). **Panel C.** Schematic representation of a tail-artery-transection assay (TAT). Amount of blood shed by hVWD1 (n=19) and control mice (n=8) during 30 minutes. **Panel D.** Representative bleeding profiles. Filled and empty bars as in B. **Panel E.** Schematic representation of a tail-clip assay and of the severed vessels. Amount of blood shed by hVWD1 (n=26) and control (n=13) mice during the 30-minute experimental time. **Panel F.** Time of first bleeding arrest upon the injury in the two groups of mice. **Panel G.** Schematic representation of a saphenous vein puncture assay. The number of clots formed upon the first incision in hVWD1 (n=13) and control (n=17) mice in 30 minutes.

A,C, E-G. Grey bars indicate mean±SD. Statistical analysis: A, E-G Mann-Whitney test; C Unpaired two-tailed Student's t-test

Figure 4. Ferric chloride-induced thrombus formation.

Panel A. Carotid artery blood flow measured post-$FeCl_3$-induced endothelial damage in hVWD1 (purple) and control (yellow) mice. Initial blood flow was similar in all mice and set at 100% for normalization purposes. The graph indicates average curves (colored lines) and SD (filled area), n=6 per group of mice. **Panel B.** Statistical analysis was performed by comparing the area under the curve (AUC) of individual curves for hVWD1- and control-mice. **Panel C.** Occlusion times were

measured (an occlusive event was indicated by flow < 0.2ml/min for a minimum of 10 min). **Panel D.** Schematic representation of the in vivo thrombus-formation model. Ferric chloride was administered by gentle deposition of a wet filter paper on the exposed vessel (white rectangle) for 2 minutes. The paper was then removed and the probe placed at the same position for flow monitoring.

B-C. Grey bars indicate mean±SD. Statistical analysis: B-C Mann-Whitney test

AUC: area under the curve, a.u.: arbitrary unit

Figure 5. Recombinant human VWF administration restores haemostasis in hVWD1 mice

Panel A. VWF antigen levels in hVWD1 mice before (purple) and 5 minutes post (magenta) r-hVWF administration (n=6). **Panel B.** Representative multimer profiles in 1.5% agarose gel. Fluorescent detection. Similar total amount of VWF loaded in consecutive lanes corresponding to samples collected from the same mouse (6-10ng). **Panel C.** Densitometric analysis of multimers in B. Profiles on the left are before- and profiles on the right are post-r-hVWF infusion. **Panel D.** Amount of blood shed in 30 minutes by control (n=13, yellow), untreated hVWD1 (n=26, purple) and treated hVWD1 mice (n=7, magenta).

A-D. Grey bars indicate mean±SD. Statistical analysis: A. Paired two-tailed Student's t-test. D. One-way ANOVA with Dunnett correction for multiple comparisons. *low* indicates VWF-LowMWMs and *high* indicates HighMWMs.

Figure 6. Histamine-induced endothelial degranulation rapidly restores haemostasis in hVWD1 mice

Panel A. VWF antigen levels in hVWD1 mice before (purple) and 30 minutes post (blue) histamine administration (n=15). Levels of individual mice are indicated in the inset. **Panel B.** Representative multimer profiles in 2% (left) or 1.5% (right) agarose gels. Colorimetric detection. Similar total amount of VWF (15-20ng) loaded in each consecutive lane. White space separates two distinct gels. **Panel C.** Densitometric analysis of multimers in B. Profiles of samples collected from the same mouse, before (grey) and post- (black) histamine infusion are superposed. **Panel D.** Amount of blood shed in 30 minutes by control (n=13, yellow), untreated hVWD1 (n=26, purple) and treated hVWD1 mice (n=10, blue).

A-D. Grey bars indicate mean±SD. Statistical analysis: A. Paired two-tailed Student's t-test. D. One-way ANOVA with Dunnett correction for multiple comparisons. *low* indicates VWF-LowMWMs and *high* indicates HighMWMs.

Figure 7. KB-V13A12 modulates VWF levels and restores haemostasis in hVWD1 mice

Panel A. VWF antigen levels in hVWD1 mice before and post KB-V13A12 (n=15-17, green) or control/KB-V13AT02 (n=3-4, grey) administration at indicated time points. **Panel B.** Representative multimer profiles in 2% agarose gel. Colorimetric detection. M9-M10 non-standard sample dilution, ≈13ng of VWF. M11-M12. standard sample dilution 10-30ng of VWF. **Panel C.** Densitometric analysis of multimers in B. Profiles on the left are before- and profiles on the right are three days post-KB-V13A12 infusion. **Panel D.** Amount of blood shed in 30 minutes by control (n=13, yellow), untreated hVWD1 (n=26, purple) and treated hVWD1 mice (n=9, green).

A. Dots indicate mean±SD. D. Grey bars indicate mean±SD. Statistical analysis: A. Two-way ANOVA. (P values in green: VWF:Ag levels in KB-V13A12 receiving mice compared to T0. P values in black: VWF:Ag levels in KB-V13A12- versus KB-V13AT02-receiving mice at every time point.) D. One-way ANOVA with Dunnett correction for multiple comparisons. *low* indicates VWF-LowMWMs and *high* indicates HighMWMs.

Figure 1

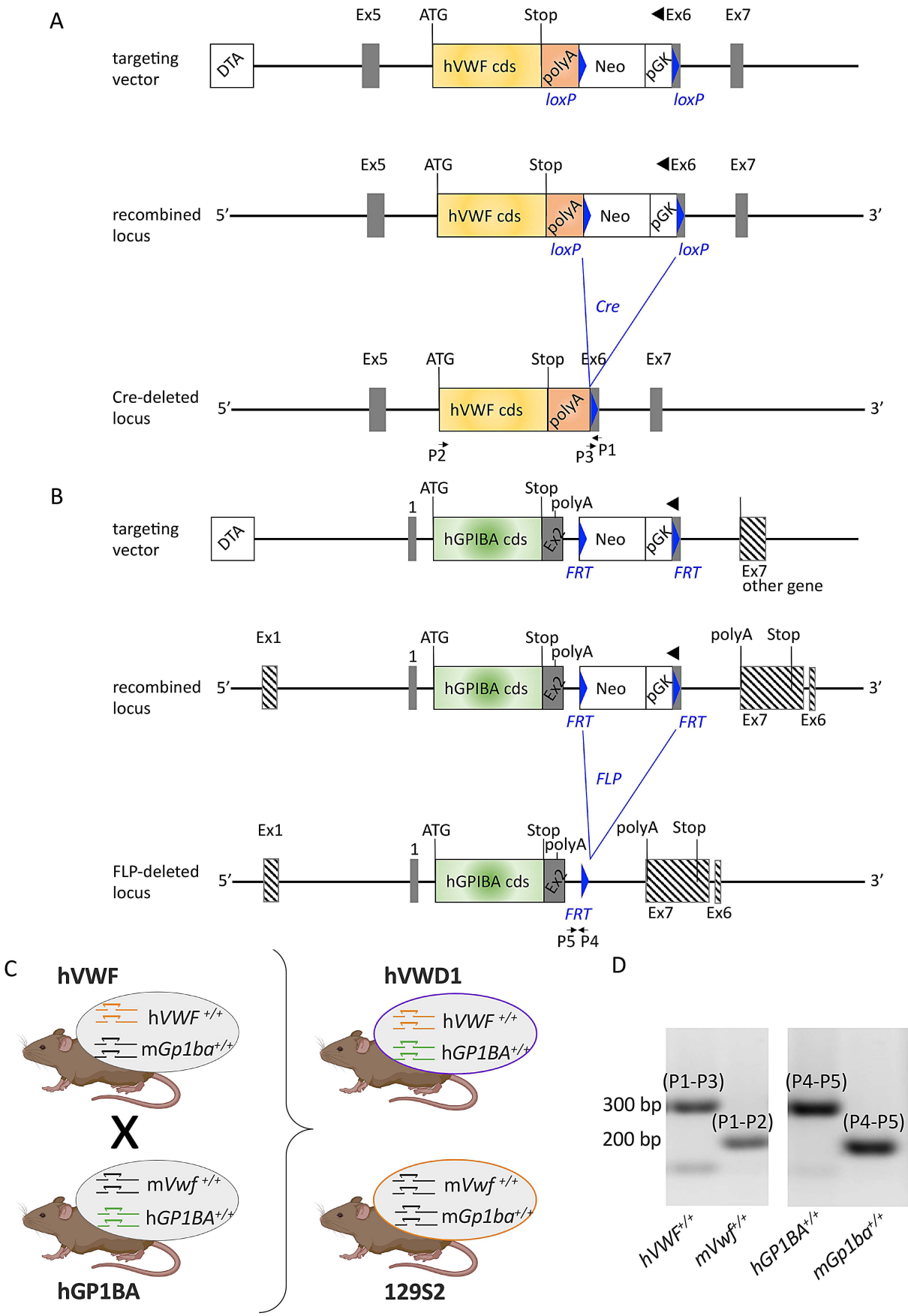
A
targeting vector
DTA
Ex5
ATG
Stop
Ex6
Ex7
hVWF cds
polyA
Neo
pGK
loxP
loxP
recombined locus
5'
3'
Cre
Cre-deleted locus
P2
P3
P1
B
hGPIBA cds
Ex2
FRT
FRT
Ex7
other gene
Ex1
FLP
FLP-deleted locus
P5
P4
C
hVWF
hVWD1
hVWF +/+
mGp1ba+/+
hGP1BA+/+
X
mVwf +/+
hGP1BA
129S2
D
(P1-P3)
(P1-P2)
(P4-P5)
(P4-P5)
300 bp
200 bp
hVWF+/+
mVwf+/+
hGP1BA+/+
mGp1ba+/+

Figure 2

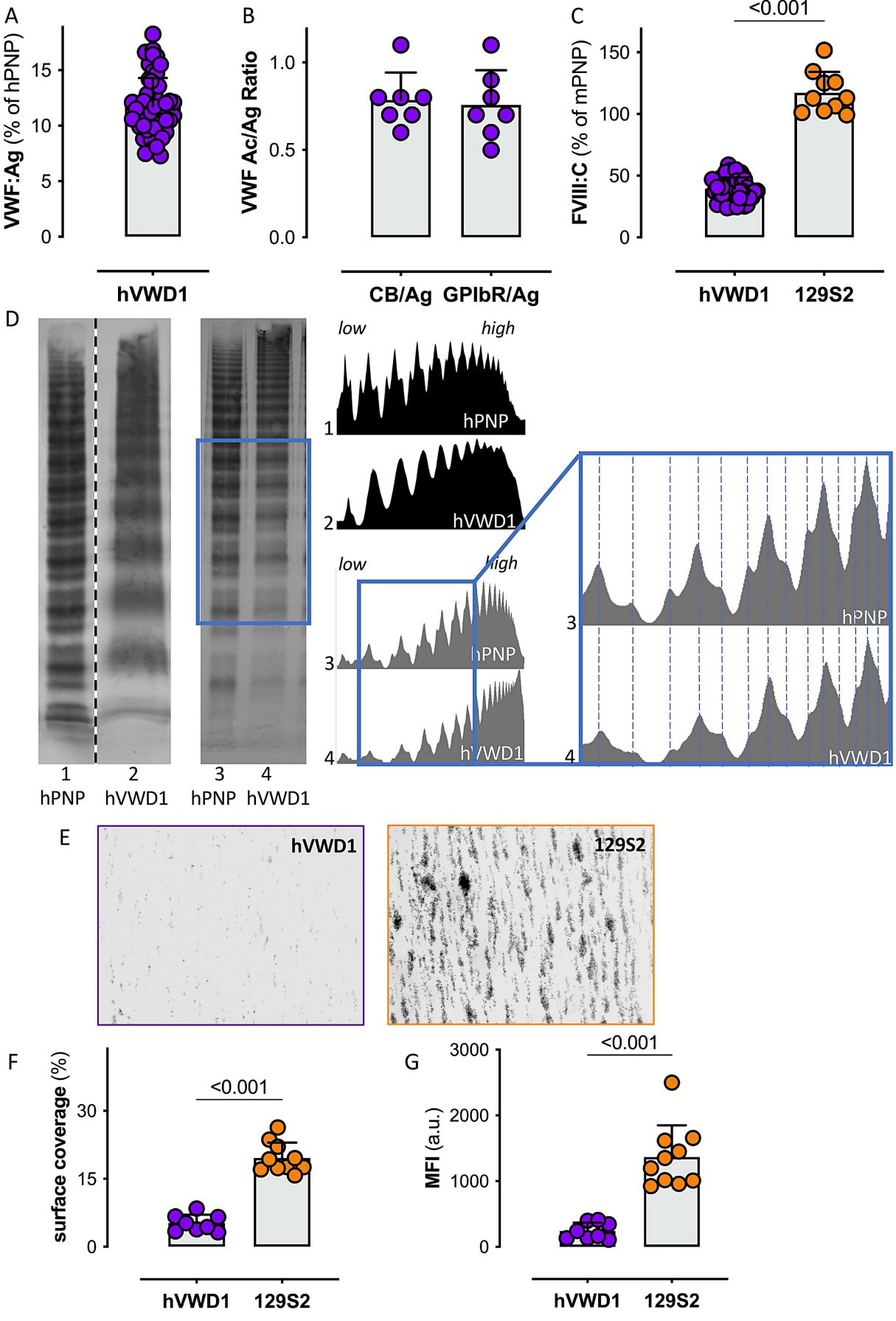
A
VWF:Ag (% of hPNP)
15
10
5
0
hVWD1
B
VWF Ac/Ag Ratio
1.0
0.5
0.0
CB/Ag
GPIbR/Ag
C
<0.001
FVIII:C (% of mPNP)
150
100
50
0
hVWD1
129S2
D
low
high
1
hPNP
2
hVWD1
low
high
3
hPNP
4
hVWD1
3
hPNP
4
hVWD1
1
hPNP
2
hVWD1
3
hPNP
4
hVWD1
E
hVWD1
129S2
F
surface coverage (%)
30
15
0
<0.001
hVWD1
129S2
G
MFI (a.u.)
3000
2000
1000
0
<0.001
hVWD1
129S2

Figure 3

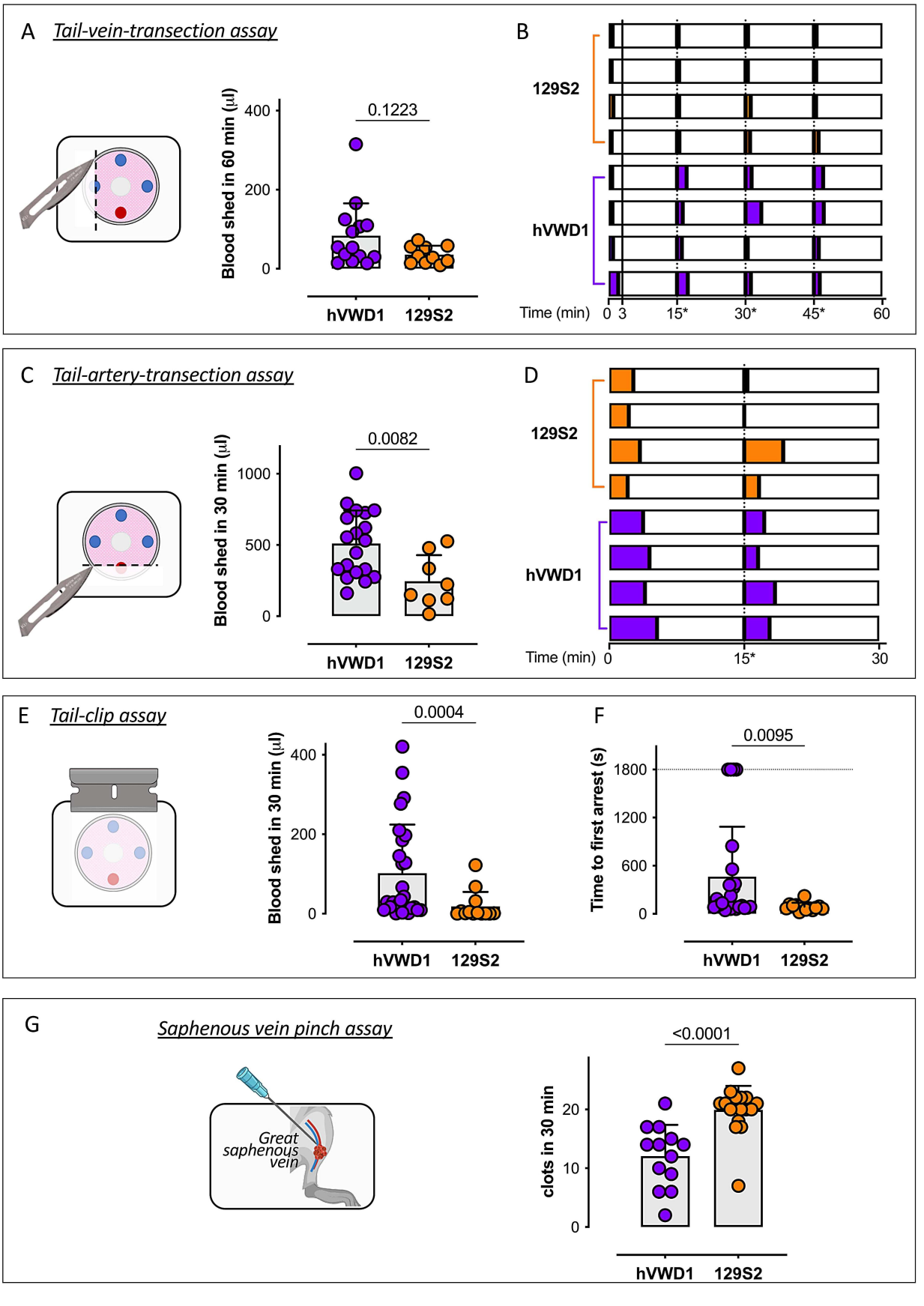
A Tail-vein-transection assay
Blood shed in 60 min (µl)
400
200
0
0.1223
hVWD1
129S2
B
129S2
hVWD1
Time (min)
0 3
15*
30*
45*
60
C Tail-artery-transection assay
Blood shed in 30 min (µl)
1000
500
0
0.0082
hVWD1
129S2
D
129S2
hVWD1
Time (min)
0
15*
30
E Tail-clip assay
Blood shed in 30 min (µl)
400
200
0
0.0004
hVWD1
129S2
F
Time to first arrest (s)
1800
1200
600
0
0.0095
hVWD1
129S2
G
Saphenous vein pinch assay
Great saphenous vein
clots in 30 min
20
10
0
<0.0001
hVWD1
129S2

Figure 4

Thrombosis model

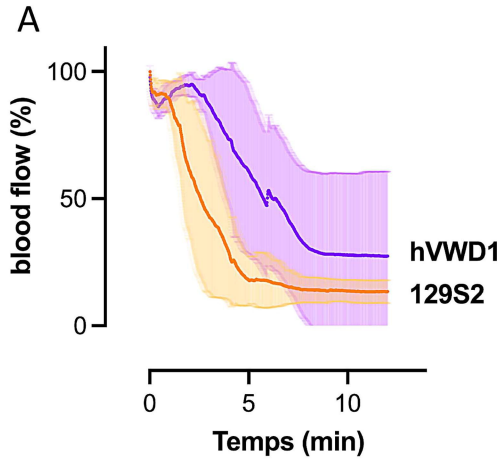

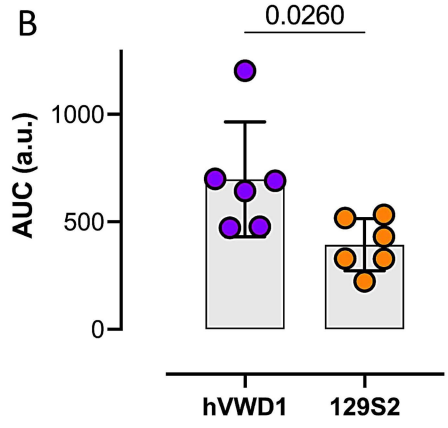

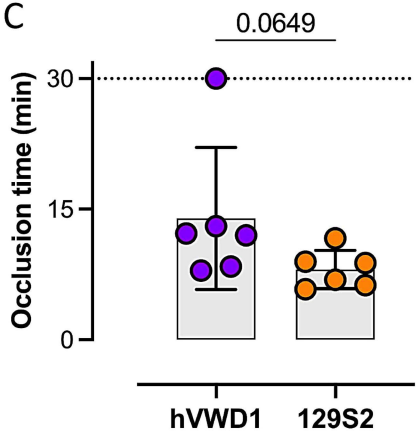

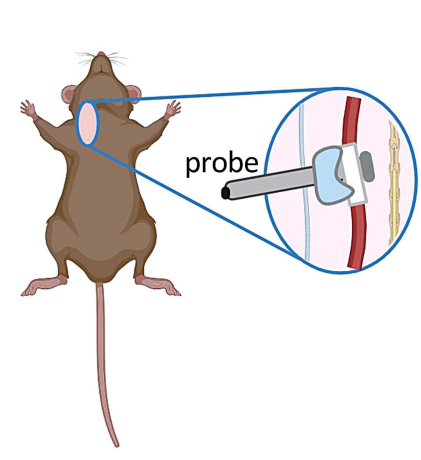

Figure 5

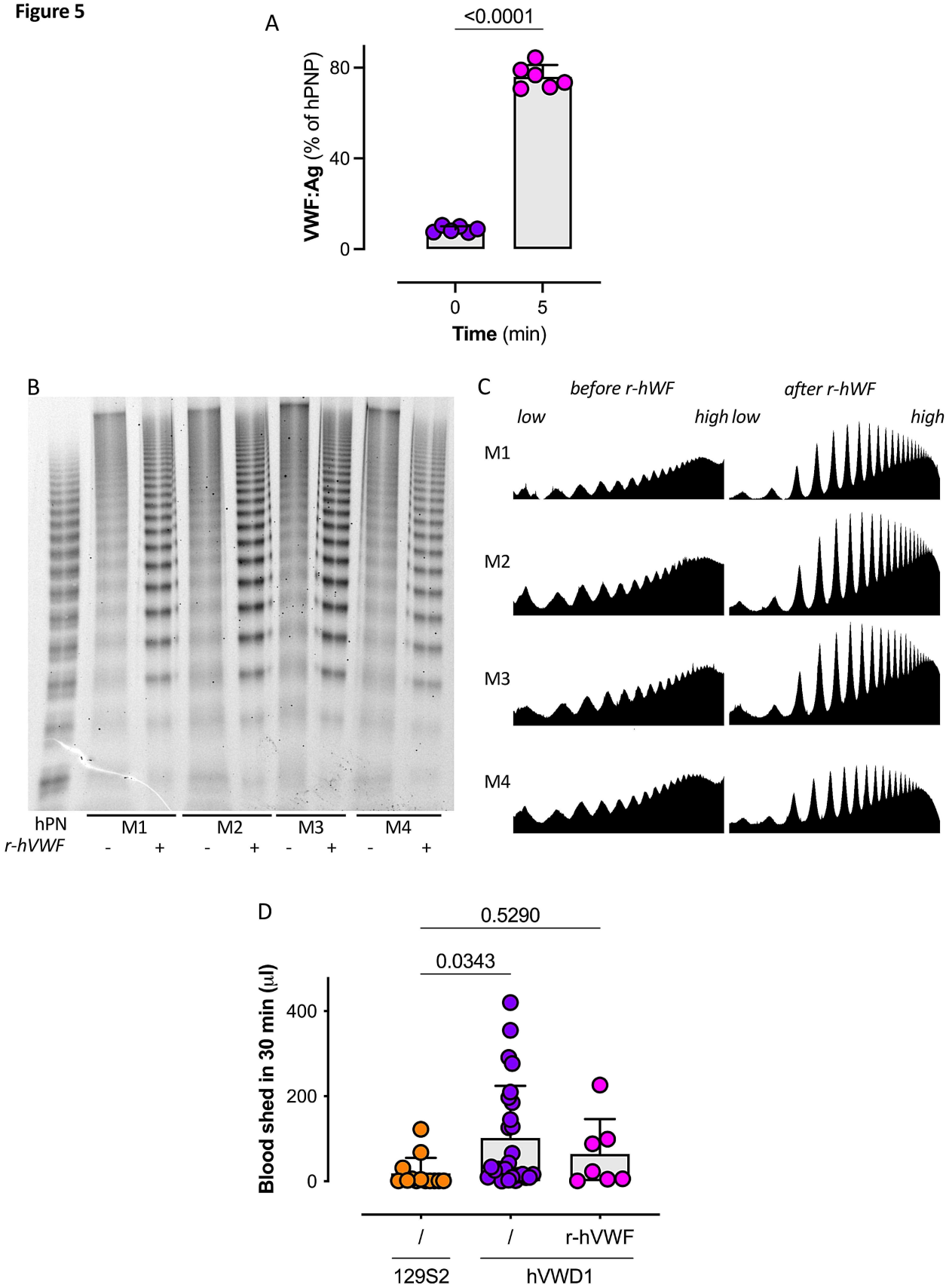
A
<0.0001
VWF:Ag (% of hPNP)
80
40
0
0
5
Time (min)
B
hPN
r-hVWF
M1
M2
M3
M4
- + - + - + - +
C
before r-hWF
after r-hWF
low
high low
high
M1
M2
M3
M4
D
0.5290
0.0343
Blood shed in 30 min (µl)
400
200
0
/
/
r-hVWF
129S2
hVWD1

Figure 6

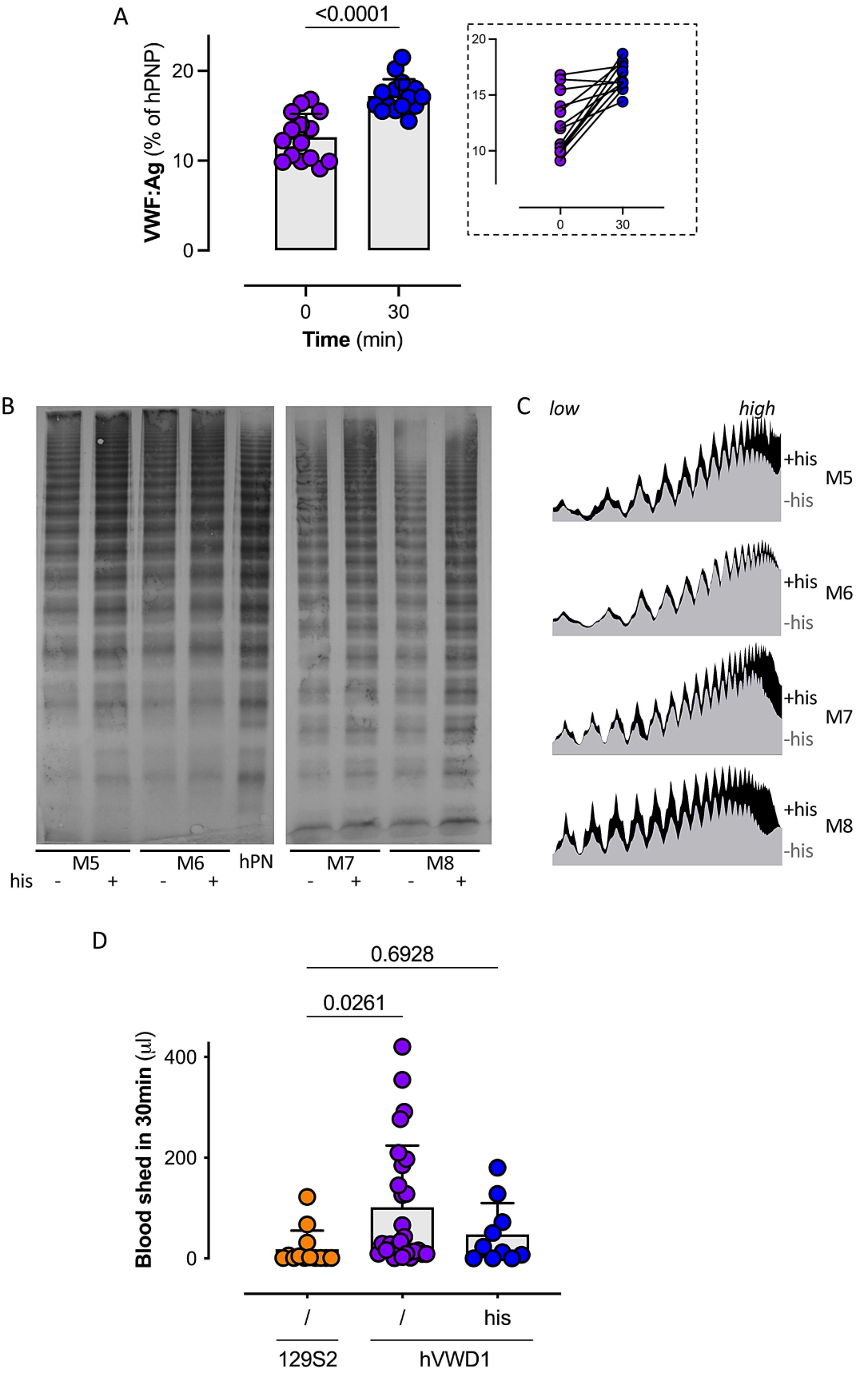
A
<0.0001
VWF:Ag (% of hPNP)
20
10
0
0
30
Time (min)
20
15
10
0
30
B
M5
M6
hPN
M7
M8
his - + - + - + - +
C
low
high
+his
-his
M5
M6
M7
M8
D
0.6928
0.0261
Blood shed in 30min (µl)
400
200
0
/
/
his
129S2
hVWD1

Figure 7

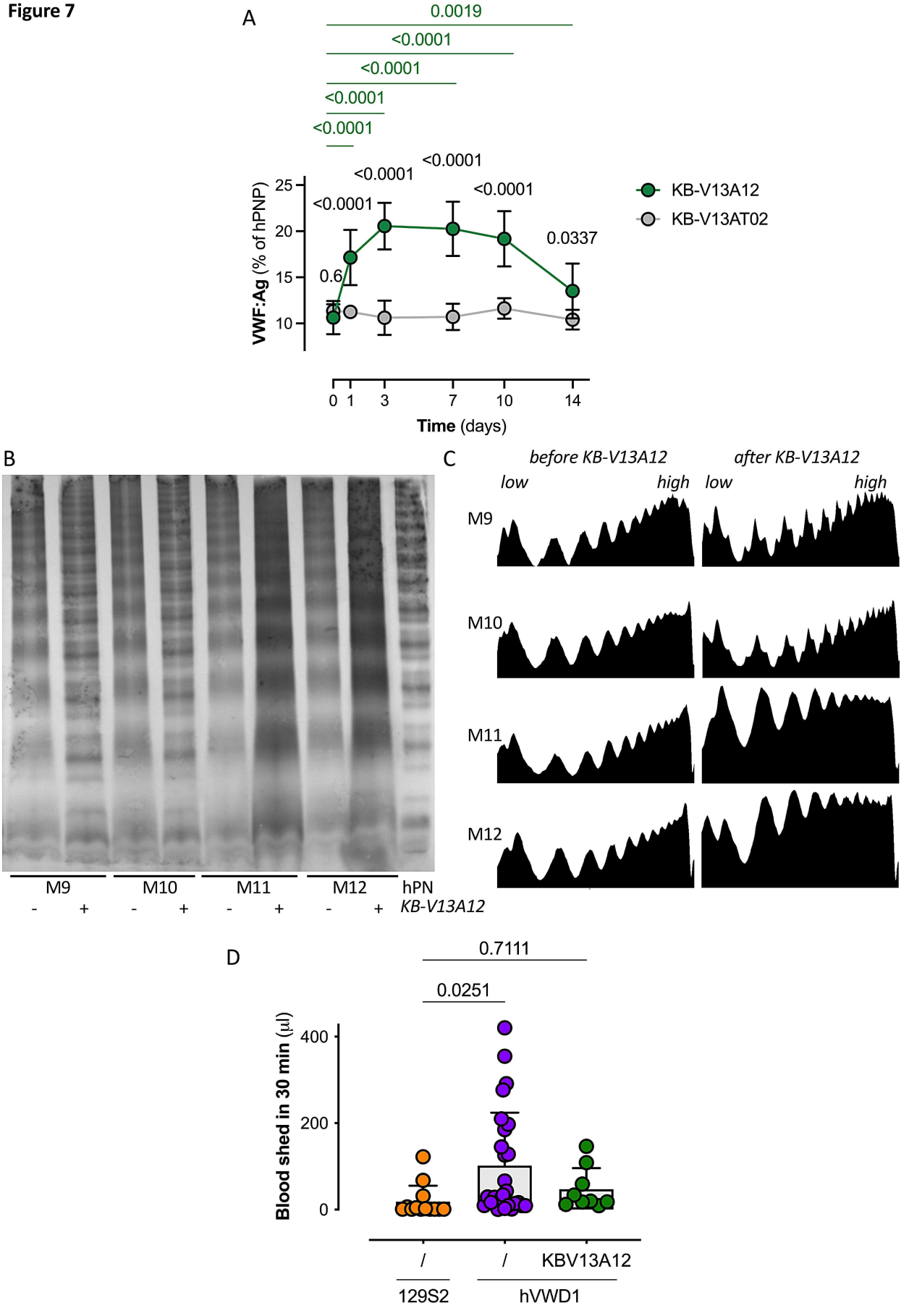
A
0.0019
<0.0001
<0.0001
<0.0001
<0.0001
<0.0001
<0.0001
<0.0001
<0.0001
0.0337
0.6
VWF:Ag (% of hPNP)
25
20
15
10
0 1 3 7 10 14
Time (days)
KB-V13A12
KB-V13AT02
B
M9 M10 M11 M12 hPN
- + - + - + - + KB-V13A12
C
before KB-V13A12
after KB-V13A12
low high low high
M9
M10
M11
M12
D
0.7111
0.0251
Blood shed in 30 min (µl)
400
200
0
/ / KBV13A12
129S2 hVWD1

Supplementary information

"A fully humanized von Willebrand disease type 1 mouse model as unique platform to investigate novel therapeutic options"

McCluskey G., Heestermans M, et al.

Animal and ethic statement

Housing and experiments were done in accordance with French regulations and the experimental guidelines of the European Community. This project (number APAFIS #32699-2021081611421076 v1) was approved by the local ethical committee of Université Paris-Saclay (comité d'éthique en expérimentation animale no. 26). Males and females were used throughout the study (8-14 weeks old). Mice used in this study had a specific pathogen free (SPF) health status and were housed in ventilated, enriched cages with food and beverage *ad libitum*.

Engineering of hVWD1 mice

Transgenic mice expressing human (h)VWF and hGPIbα instead of the corresponding murine proteins were engineered in a pure 129S2 (129S2/SvPasCrl) genetic background expressing fully functional ADAMTS13.[1,2] For this purpose, the generation of knock-in mice for each of the protein of interest (hVWF and hGPIbα) was entirely outsourced to genOway (Lyon, France). To engineer the 129S2Crl-*Vwf*$^{-/-}$-Tg(*VWF)* mice (Figure 1A), the cDNA of h*VWF* followed by a *hGH* (human growth hormone) polyadenylation site, was inserted within the murine *Vwf* gene, in frame with the endogenous ATG. Such transgene insertion resulted in the inactivation of the murine *Vwf* gene and expression of the h*VWF* gene under the control of endogenous regulatory sequences. The common single nucleotide variant c.2365A>G (p.T789A), associated with increased VWF levels,[3–5] was inserted within the *hVWF* cDNA. To engineer the 129S2Crl-*Gp1ba*$^{-/-}$-Tg*(GP1BA)* mice (Figure 1B), the murine coding sequence was replaced by the human cDNA, without additional changes to the regulatory sequences. Homozygous mice for both humanized proteins, referred to as hVWF- and hGP1BA mice, were then crossed to generate homozygous double knock-in mice 129S2Crl-*Vwf*$^{-/-}$-Tg(*VWF),Gp1ba*$^{-/-}$-Tg*(GP1BA),* referred to as hVWD1 mice. Results presented in this study pertain to hVWD1 mice and littermate controls (named 129S2 or control mice throughout the manuscript).

Genotyping was performed using DNA extracted by ear biopsies using a classic NaOH-based protocol and PCR amplification (KAPA2G Fast Genotyping Mix, Kapa Biosystems, Wilmington, MA) with various primer combinations (Table S1). PCR products were separated by electrophoresis on 1.5% agarose gels (Figure 1D).

Murine blood collection and counts

Blood sampling was performed under isoflurane anesthesia (2-2.5%) with air 0.8L/minute via retro-orbital puncture using glass capillary tubes, unless otherwise specified. Blood was collected in 10% vol/vol triNa-citrate (0.138M) for plasma preparation (obtained by centrifugation 1500xg, 20 minutes at room temperature) or in 10% vol/vol EDTA 50 mM for blood counts. Blood counts were determined with an automatic cell counter (Scil Vet ABC Plus, Horiba Medical, France).

VWF assays

VWF antigen levels were measured in mouse plasma with an in-house enzyme-linked immunosorbent assay, essentially as previously described,[6] using a pair of polyclonal rabbit anti-VWF antibodies (Agilent Technologies, Les Ulis, France). A human pooled normal plasma (Cryopep, Montpellier, France) was used as reference and a standard human plasma (Siemens, Erlangen, Germany) was used as inter-assay control. Alternatively, a pool of monoclonal anti-human VWF antibodies previously produced and recognizing only human VWF has been used as coating antibody (5μg/ml).

VWF activity was assessed in an ELISA-based collagen binding test (VWF:CB) and an automated platelet-based assay (VWF:GPIbR). For VWF:CB, VWF binding to fibrillar, human placental type III collagen (SouthernBiotech, Birmingham, USA, 5ug/ml) was detected using a polyclonal rabbit anti-VWF antibody. A human pooled normal plasma was used as reference. Immunoturbidimetric VWF:GPIbR was assessed in a ACL TOP 550 (reagents and analyzer, Werfen, Bedford USA).

VWF multimer profiling was performed essentially as previously described[7] in 1.5 or 2% agarose gels. VWF was detected with an in-house alkaline phosphatase-conjugated polyclonal anti-VWF and colorimetric alkaline phosphatase-substrate kit (Bio-Rad Laboratories, Hercules, CA, USA). Membranes were imaged with a G:BOX Chemi XT16 Image Systems (Syngene, Bangalore, India).

Alternatively, VWF multimers were separated in 1.5% agarose gels and visualized by an in-gel staining technique.[8] Briefly, gels were fixed in 5% acetic acid/50% isopropanol 30 minutes, washed twice in H_20 and stained four hours with primary antibody (polyclonal rabbit anti-VWF 0.28mg/l in TBS/0.05% Tween-20/5% BSA). After overnight washing in TBS/0.05% Tween-20, gels were incubated four hours with secondary antibody (Amersham CyDye 800 goat-anti-rabbit 0.07mg/l in TBS/0.05% Tween-20/5% BSA) and washed overnight (TBS/0.05% Tween-20). After an additional wash in TBS, gels were scanned at 800nm with an infrared image system (Amersham Typhoon NIR Plus, Cytiva).

Multimer profiles were analyzed using the Gel Analyzer tool of ImageJ (version 1.53).

FVIII activity assay

FVIII activity was measured in a chromogenic assay using the Biophen FVIII-assay kit (Hyphen, Neuville-sur-Oise, France) as instructed. A murine pooled plasma from 129S2 (wild-type) mice was used as reference.

Parallel plate flow perfusion

After general anesthesia with ketamine/xylazine (200mg/kg and 20mg/kg, respectively) blood was collected from mice by intra-cardiac puncture in unfractionated heparin (40U/ml) and PPACK (80μM). Anticoagulated blood was diluted in 1.2 volumes of Tyrode's buffer (137 mM NaCl, 2 mM KCl, 0.3 mM NaH_2PO_4, 5 mM dextrose, 5 mM N-2-hydroxyethylpiperazine-N0-2-ethanesulfonic acid, 12 mM $NaHCO_3$, pH 7.3) and labeled with rhodamine 6G (10 μg/mL). Thrombus formation was evaluated using a Maastricht flow chamber connected to a syringe pump (KD Scientific) in a whole-blood perfusion assay on a fibrillar collagen matrix (50μg/ml horse type I collagen, Chrono-Par, Mast Diagnostic, Amiens, France, incubated over night at 4°C) under arterial shear conditions (shear rate of 3000 s^{-1}). Platelet adhesion was measured after 3 min of blood perfusion followed by 2 min of washing with Tyrode's buffer. Every perfusion was performed with blood from a single mouse donor. Immediately after each perfusion, 20 images were randomly acquired using an inverted epifluorescence microscope (Nikon Eclipse TE2000-U) equipped with a PlanFluor 20x/0.50 objective (Nikon). The percentage of surface covered by fluorescent platelets and the mean fluorescent intensity were calculated using ImageJ (1.53k). Single dots in the graph represent individual mice (average value of 20 images).

KB-V13A12 production and administration

Single domain antibodies (SdAbs) against VWF were generated as described[9] by screening of a proprietary immune sdAb library obtained after immunization of a single llama with VWF. The sdAb KB-V13 (formerly KB-VWF-013) has been previously characterized.[10] The anti-albumin nanobody KB-OptiAlb12 is a llama-derived nanobody that displays high-affinity binding (<5 nM) to both human and murine albumin. The chemically synthesised KB-V13A12 sequence was cloned into a pHEN6-plasmid, expressed in competent E.coli WK6 bacteria and purified by affinity chromatography using a HiTrap TALON column (GE Healthcare, Buc dans les Yvelines, France). A control bispecific sdAb (KB-V13AT02) was synthetized by cloning the KB-V13 linked to the previously described KB-AT02 against antithrombin.[11]

Purified bispecific sdAbs were administered subcutaneously (5mg/kg body weight) to isoflurane anesthetized mice. Blood was collected at the indicated time points for VWF antigen quantification

and multimer analysis. A separate group of mice was treated with KB-V13A12 and haemostasis was assessed 3 days post injection in a tail-clip assay, generally by a person blind to the treatment.

Tail-vein-transection model and tail-artery-transection model

In the tail-vein-transection (TVT) assay, an incision is applied to only one lateral tail vein. TVT was conducted as described[12] and consisted in a standardized 0.7 mm deep wound obtained sliding the blade of a scalpel through the transection groove of a customized metal template. Mice were anesthetized with isofluorane and warmed on a heating pad throughout the experimental procedure. If mice were not actively bleeding at 15-, 30- and 45-minute post-injury, the wound was challenged by gently wiping it twice in the distal direction. Blood shed by the wound after the injury was collected in isotonic saline solution (0.9% NaCl) for 60 minutes and quantified measuring haemoglobin optical density at 416 nm after red blood cell lysis.

Every spontaneous arrest of the bleeding was recorded. Bleeding profiles indicate bleeding (filled bars) and non-bleeding (empty bars) time periods throughout the 60-minute observation time.

The tail-artery-transection (TAT) model consists of a modified TVT model in which the ventral tail artery was transected using the same customized templates. Experimental time was set at 30 minutes.

Tail-clip model

A classic tail-clip assay was performed essentially as described.[13,14] Briefly, 3 mm of the distal tip of the tail of anesthetized mice (ketamine and xylazine, 100 and 10mg/kg, respectively) was amputated using a razor blade. Blood shed by the injury was collected in isotonic saline solution constantly warmed at 37°C for 30 min and quantified measuring haemoglobin optical density.

Histamine (Merck, Fontenay Sous Bois, France) was administered intraperitoneally (13 μmol/kg body weight)[15] 30 minutes prior to tail-clip or blood collection. The 30-minute time point was selected based on preliminary experiments showing that highest VWF levels were observed 30 minutes post-histamine administration (not shown).

Recombinant human VWF containing intact-VWF only (r-hVWF, Veyvondi, Takeda) was administered intravenously (50U/Kg body weight) 5 minutes before tail-clip or blood collection.

Saphenous vein puncture model

The saphenous vein puncture model was conducted essentially as described[16,17] on mice anesthetized with ketamine/xylazine (ketamine and xylazine, 100 and 10mg/kg, respectively) and constantly warmed on a heating pad. Briefly, a large saphenous vein was exposed and pierced with a 23G needle at equal distance between the femoral vein and the distal branches. The first clot was then gently

removed by wiping and a longitudinal incision of ~1mm was made on the exposed side of the vessel using micro-scissors. The blood leaking from the incision was gently absorbed until haemostasis occurred and blood clots were removed using a gauze swab humidified with 0.9 % NaCl. The number of clots formed during 30 minutes from the first incision was recorded.

In vivo ferric chloride-induced thrombus formation

Mice were anesthetized with ketamine/xylazine and the left carotid artery exposed. Thrombus formation was chemically initiated by applying for 2 minutes a filter paper (0.5x3mm) previously soaked in a freshly prepared $FeCl_3$ solution (15%). Blood flow was measured shortly before and after the $FeCl_3$-induced damage by using a Transonic console with perivascular flowmeter module equipped with a nanoprobe for transit-time ultrasound flow measurement (T402 console, TS420 flowmeter, MA0.5PSB probe, Transonic Europe, Elsloo, The Netherlands)[18]. Data were digitally acquired with a PowerLab 2/26 device and a LabChart 8.0 software (ADInstruments, Oxford, UK). Measurements were stopped 10-minutes post-occlusion, indicated by blood flow < 0.2ml/min for at least 10-consecutive minutes; or at 60 minutes in mice that did not occlude.

Platelet αIIbβ3 activation, α-granule release and surface receptor expression

Platelet αIIbβ3 activation and α-granule release studies were conducted in whole blood as previously described.[18,19]

Murine and human GPIbα expression was studied in murine platelets by flow cytometry as previously described[19]. Briefly, whole blood was incubated with an anti-murine GPIX-FITC antibody (clone Xia.B4, Emfret Analytics, Eibelstadt, Germany), an anti-murine GPIbα-PE (clone Xia.G5, Emfret) and an anti-human GPIbα-APC (clone HIP1, BD Biosciences, France).

Mouse platelet lysates

Platelet lysates were prepared as described[19] in the absence of platelet-activators.

Statistical analysis

All data are presented as mean±standard deviation (mean±SD). Number (n) refer to the number of animals. The statistical analysis was performed using GraphPad Prism 10 software for Mac (La Jolla, California, USA). One-way analysis of variance (1-way ANOVA) followed by Tukey's or Dunnett's multiple comparison test was performed when comparing multiple groups. Pairwise analysis was performed using the unpaired two-tailed Student's t-test. Two-way analysis was performed for two factors comparisons. $P<0.05$ was considered as statistically significant.

Table S1. Genotyping primers

			PCR product size (bp)	
		Sequence 5'-3'	**Wild-type allele**	**Knock-in allele**
VWF	**P1(common)**	CAAGTCTAACACAGATGGAGCACAGGTGAGT	**P1-P2 218**	**P1-P3 288 (+ 9370)**
	P2	GGACGGTGAGAACCAGCTCATTTCCT		
	P3	CTTGGCACTGTCCTCTCATGCGTTG		
GP1BA	**P4**	ACTCAAACCCAACAGGCTGCCAC	**P4-P5 226**	**P4-P5 305**
	P5	GCAGGTAGGACACCTCCACCTTAGTGA		

Figure S1

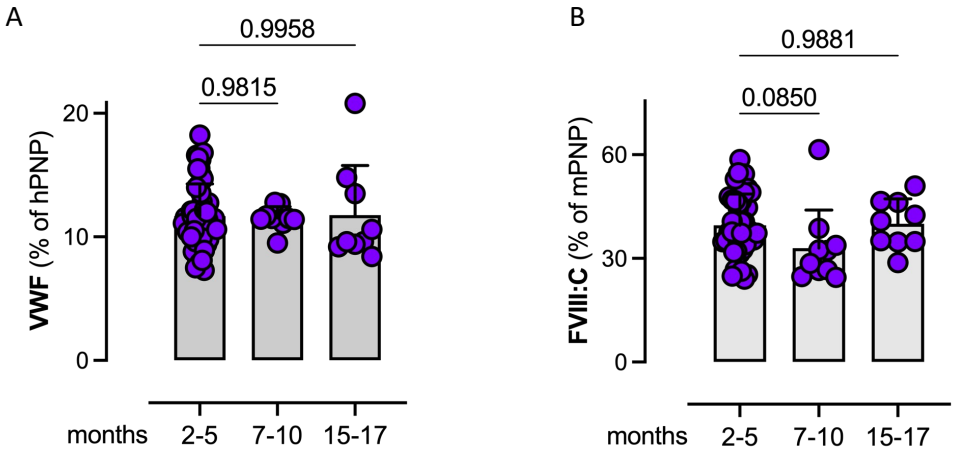

Supplemental Figure S1. VWF and FVIII levels over time

Panel A. VWF antigen levels and **Panel B.** FVIII activity levels in hVWD1 mice over a 15/17-month experimental time period. Data at 2/5 months as in Figure 1A and B.

A-B. Grey bars indicate mean±SD. Statistical analysis: One-way ANOVA with Dunnett correction for multiple comparisons.

Figure S2

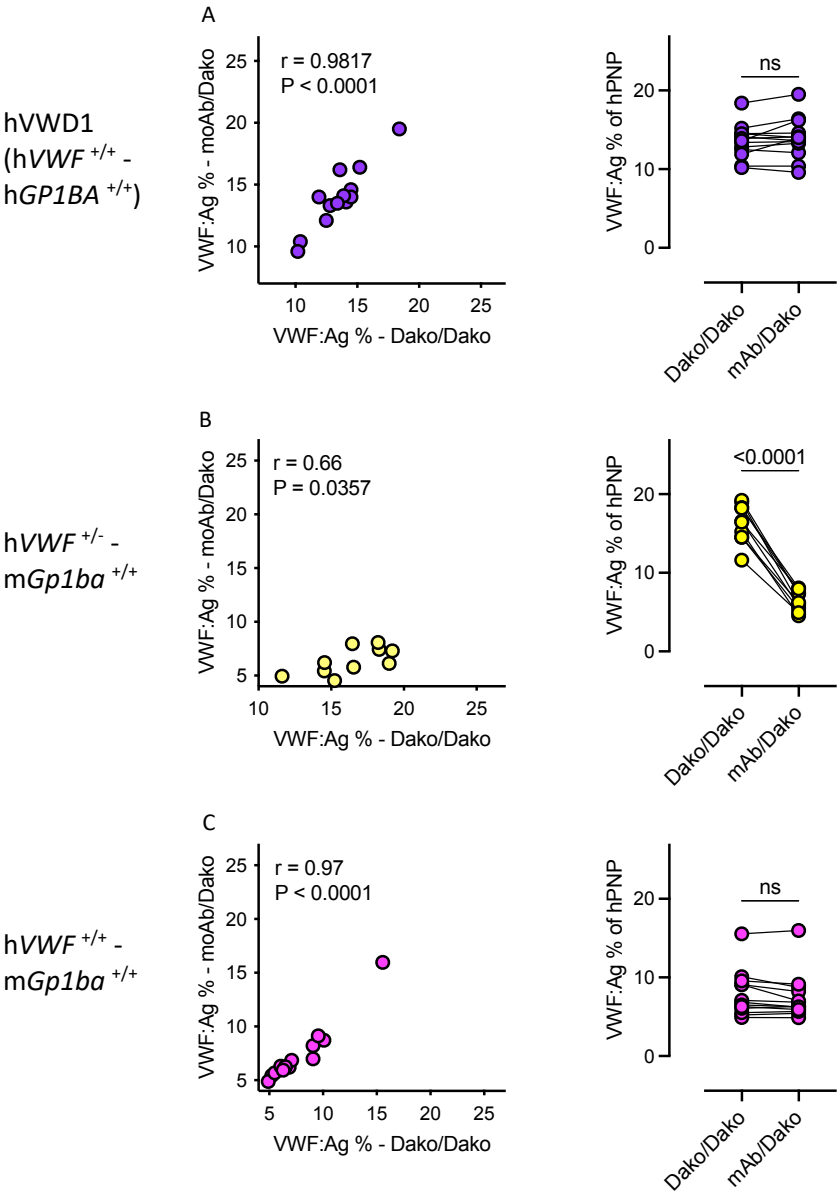

Supplemental Figure S2. VWF expression

VWF antigen levels were measured by two assays. One used commercial polyclonal antibodies that detected both human and murine VWF (Dako/Dako) and the second used a pool of monoclonal antibodies as coating-antibody, therefore detecting only human VWF (moAb/Dako). Both assays used the same detecting antibody and the same human-pooled plasma as reference. To evaluate if human or human & murine VWF was expressed in engineered mice, we evaluated the correlation between plasmatic VWF antigen levels measured by the two assays (graphs on the left) and directly compared raw values obtained for the same mouse in the two assays (graphs on the right). Data were measured for hVWD1 mice, homozygous for hVWF and hGPIbα (h*VWF* $^{+/+}$/h*GP1BA*$^{+/+}$) (**A**, n=13, purple), mice heterozygous for human-murine VWF and homozygous for mGPIbα (h*VWF* $^{+/-}$/m*Gp1ba*$^{+/+}$) (**B**, n=10,

light yellow) and mice homozygous for human VWF and murine GPIbα (h*VWF* $^{+/+}$/m*Gp1ba* $^{+/+}$) (**C**, n=13, pink).

An almost perfect correlation between values obtained in the two assays was observed in mice homozygous for h*VWF* expression (h*VWF* $^{+/+}$, A purple and C pink) irrespective of GPIbα expression (human in A and murine in C). These correlations corresponded to almost identical raw values in the two antigen assays (graphs on the right), supporting the notion that these mice only express human VWF, and that engineering GPIbα has no effects on VWF expression levels.

Despite a positive correlation was still measured for VWF antigen levels measured by the two assays in plasma from heterozygous mice for VWF (B, light yellow), raw antigen levels measured in the Dako/Dako assay were roughly twice as high as those measured in the moAb/Dako assay (right), supporting the notion that heterozygous mice for VWF express both human and murine VWF.

Altogether, these data are consistent with the hypothesis that hVWD1 mice only express hVWF.

Figure S3

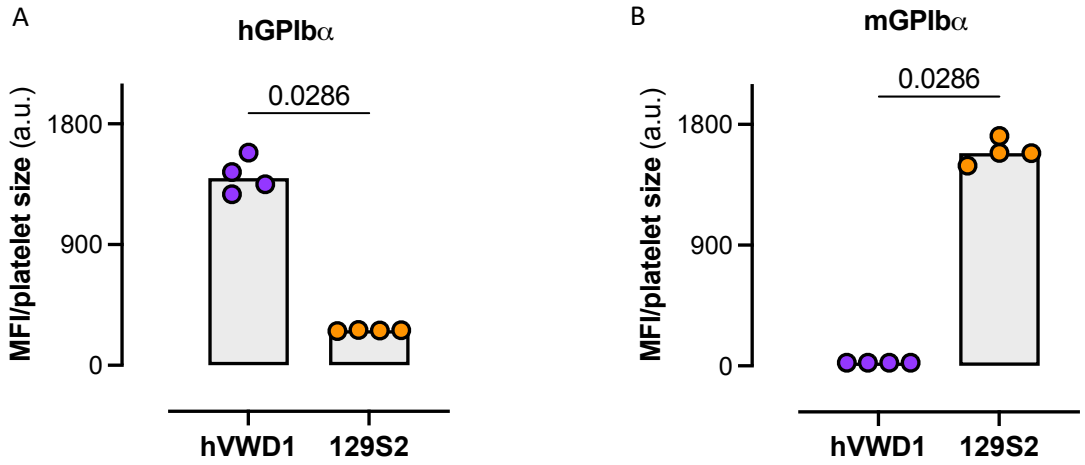

Supplemental Figure S3. Platelet surface expression of human or murine GPIbα

Platelet surface expression of human (**panel A**) or murine (**panel B**) GPIbα was confirmed by flow cytometry in hVWD1 (n=4, purple) and 129S2 (n=4, yellow) mice using specie-specific antibodies recognizing the human (anti-human GPIbα-APC) or murine (anti-murine GPIbα-PE) receptors. Histograms refer to the mean fluorescence intensity for APC (A) or PE (B) signals normalized by platelet size as measured by a veterinary counter. Platelets circulating in hVWD1 mice express human- but not murine GPIbα (purple). On the contrary, platelets circulating in 129S2 mice express murine- but not human GPIbα (yellow).

A-B Grey bars indicate mean±SD. Statistical analysis: Mann-Whitney test. Data of one representative experiment out of two, 4-8 mice per experiment. MFI: mean fluorescent intensity, a.u.: arbitrary units.

Figure S4

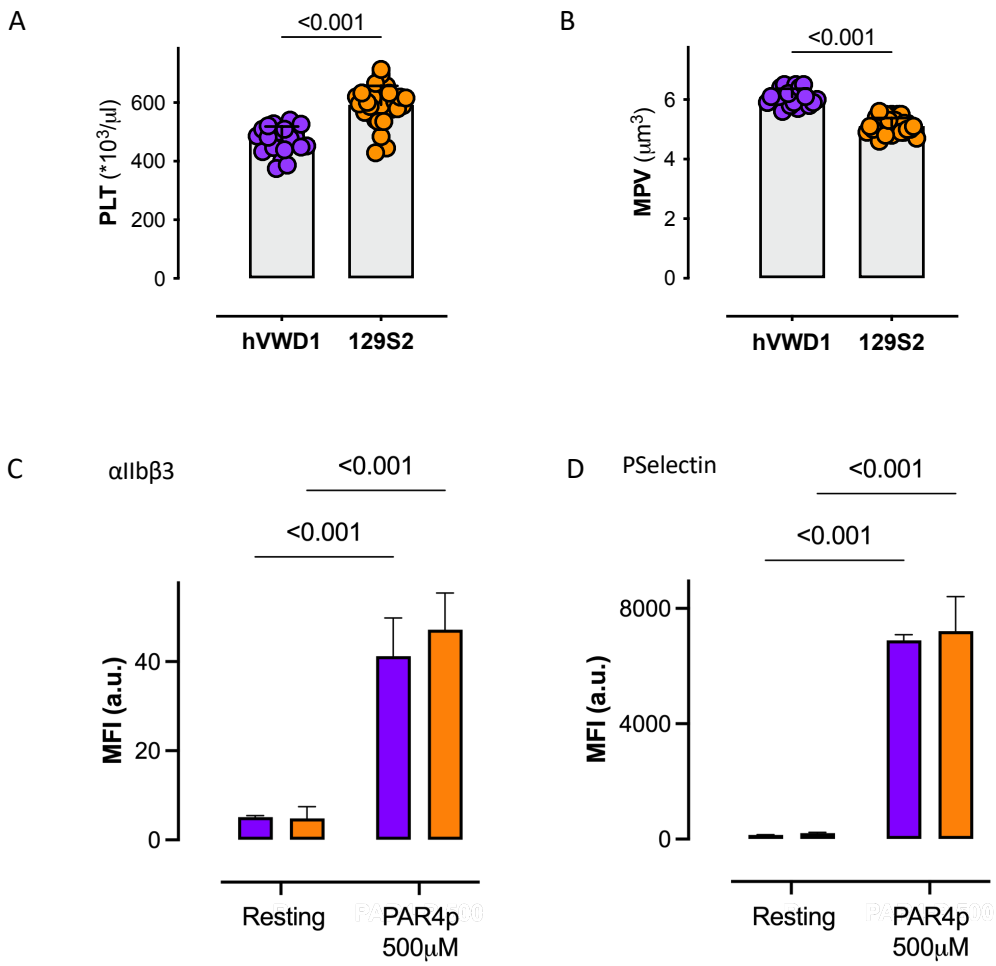

Supplemental Figure S4. Platelet studies in hVWD1 mice

Panel A. Peripheral platelet counts and **panel B.** mean platelet volume in hVWD1 (n=21, purple) and control (n=28, yellow) mice assessed in whole blood collected in 10% vol/vol EDTA 50 mM using an automatic cell counter (Scil Vet ABC Plus, Horiba Medical, France).

Panels C-D. Whole blood platelet activation. αIIbβ3 integrin activation (C) measured with JON/A-PE (Emfret Analytics, Germany) and (D) P-selectin surface expression (Rat anti-Mouse CD62p/AF647, Emfret Analytics, Germany) in resting and activated platelets (PAR4p 500µM, Bubendorf, Switzerland) from hVWD1- (n=4, purple) and control- (n=9, yellow) mice.

A-B Grey bars indicate mean±SD. Statistical analysis: A-B. two-tailed Student's t-test. C-D. two-way ANOVA with Sidak correction for multiple comparisons.

PLT: platelets, MPV: mean platelet volume, MFI: mean fluorescent intensity, a.u.: arbitrary units.

Figure S5

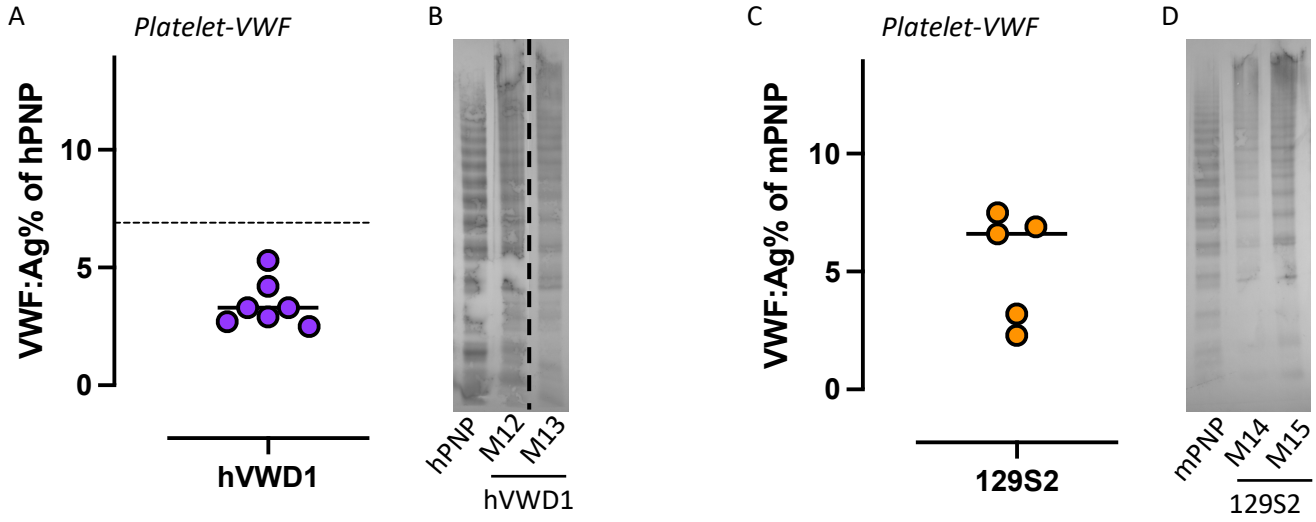

Supplemental Figure S5. Platelet VWF

Platelets were isolated from hVWD1- (purple) and 129S2-mice (yellow), washed and lysed as previously described[19]. **Panel A.** The amount of VWF in platelets from hVWD1 mice was quantified by ELISA using a human pooled normal plasma (hPNP) as reference. The values indicated in the graph refer to 10^8 platelets. The dotted line indicates VWF:Ag in 10^8 human platelets (internal data), which is consistent with data from the literature[20]. Importantly, for a direct comparison between murine hVWD1-platelets and human platelets, the difference in size and possibly in α-granules content should be taken into account, but was out of the scope of the present study. **Panel B.** Multimer profile of platelet-VWF in hVWD1 mice. As expected, platelets are enriched in HMWMs. Multimers were studied in 1.5% agarose gel by loading similar amount of VWF (≈10ng) in the hPNP, used as reference, and in two platelet lysate samples (from two individual mice, M12 and M13). The dotted line indicates non-consecutive lanes on the same gel. **Panel C.** The amount of VWF in platelets from 129S2 mice was quantified by ELISA using a murine pooled normal plasma (mPNP) as reference. The values indicated in the graph refer to 10^8 platelets. **Panel D.** Multimer profile of platelet-VWF in 129S2 mice. Multimers were performed as in B.

hPNP, human pooled normal plasma; mPNP, murine pooled normal plasma

Figure S6

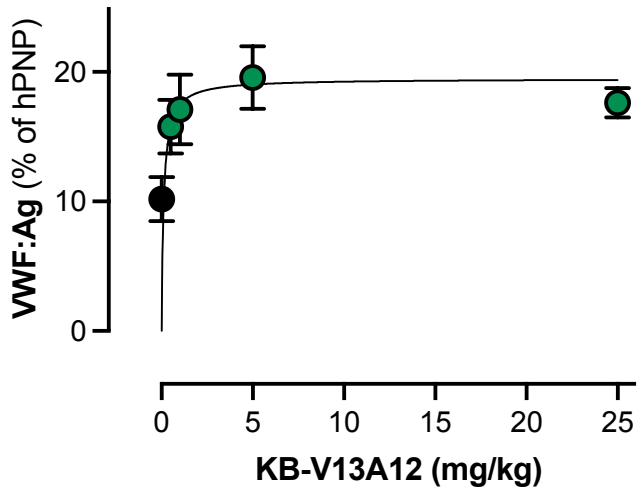

Comparisons	p value
0 vs 0.5 mg/kg	0.0002
0 vs 1 mg/kg	<0.0001
0 vs 5 mg/kg	<0.0001
0 vs 25 mg/kg	<0.0001
5 vs 0.5 mg/kg	0.0189
5 vs 1 mg/kg	0.1685
5 vs 25 mg/kg	0.2547

Supplemental Figure S6. Dose-response assessment of KB-V13A12

VWF:Ag was assessed in hVWD1 mice before (black) and 3 days post-sc administration of various doses (0.5, 1, 5, and 25 mg/kg) of KB-V13A12 (green).

Statistical analysis: One-way ANOVA with Holm-Sidak correction for multiple comparisons.

Supplementary References:

1. Banno F, Kaminaka K, Soejima K, Kokame K, Miyata T. Identification of Strain-specific Variants of Mouse Adamts13 Gene Encoding von Willebrand Factor-cleaving Protease. Journal of Biological Chemistry 2004;279(29):30896–30903.

2. Zhou W, Bouhassira EE, Tsai H-M. An IAP retrotransposon in the mouse ADAMTS13 gene creates ADAMTS13 variant proteins that are less effective in cleaving von Willebrand factor multimers. Blood 2007;110(3):886–893.

3. Flood VH, Johnsen JM, Kochelek C, et al. Common VWF sequence variants associated with higher VWF and FVIII are less frequent in subjects diagnosed with type 1 VWD. Res Pract Thromb Haemost 2018;2(2):390–398.

4. Johnsen JM, Auer PL, Morrison AC, et al. Common and rare von Willebrand factor (VWF) coding variants, VWF levels, and factor VIII levels in African Americans: the NHLBI Exome Sequencing Project. Blood 2013;122(4):590–597.

5. Mufti AH, Ogiwara K, Swystun LL, et al. The common VWF single nucleotide variants c.2365A>G and c.2385T>C modify VWF biosynthesis and clearance. Blood Adv 2018;2(13):1585–1594.

6. Lenting PJ, Westein E, Terraube V, et al. An experimental model to study the in vivo survival of von Willebrand factor. Basic aspects and application to the R1205H mutation. J Biol Chem 2004;279(13):12102–12109.

7. Groot E, Fijnheer R, Sebastian SA, de Groot PG, Lenting PJ. The active conformation of von Willebrand factor in patients with thrombotic thrombocytopenic purpura in remission. J Thromb Haemost 2009;7(6):962–969.

8. Pruthi RK, Daniels TM, Heit JA, Chen D, Owen WG, Nichols WL. Plasma von Willebrand factor multimer quantitative analysis by in-gel immunostaining and infrared fluorescent imaging. Thromb Res 2010;126(6):543–549.

9. Aymé G, Adam F, Legendre P, et al. A Novel Single-Domain Antibody Against von Willebrand Factor A1 Domain Resolves Leukocyte Recruitment and Vascular Leakage During Inflammation—Brief Report. ATVB 2017;37(9):1736–1740.

10. Muczynski V, Casari C, Moreau F, et al. A factor VIII-nanobody fusion protein forming an ultrastable complex with VWF: effect on clearance and antibody formation. Blood 2018;132(11):1193–1197.

11. Barbon E, Ayme G, Mohamadi A, et al. Single-domain antibodies targeting antithrombin reduce bleeding in hemophilic mice with or without inhibitors. EMBO Mol Med 2020;12(4):e11298.

12. Johansen PB, Tranholm M, Haaning J, Knudsen T. Development of a tail vein transection bleeding model in fully anaesthetized haemophilia A mice - characterization of two novel FVIII molecules. Haemophilia 2016;22(4):625–631.

13. Rayes J, Hollestelle MJ, Legendre P, et al. Mutation and ADAMTS13-dependent modulation of disease severity in a mouse model for von Willebrand disease type 2B. Blood 2010;115(23):4870–4877.

14. Marx I, Lenting PJ, Adler T, Pendu R, Christophe OD, Denis CV. Correction of bleeding symptoms in von Willebrand factor-deficient mice by liver-expressed von Willebrand factor mutants. Arterioscler Thromb Vasc Biol 2008;28(3):419–424.

15. Zirka G, Robert P, Tilburg J, et al. Impaired adhesion of neutrophils expressing Slc44a2/HNA-3b to VWF protects against NETosis under venous shear rates. Blood 2021;137(16):2256–2266.

16. Buyue Y, Whinna HC, Sheehan JP. The heparin-binding exosite of factor IXa is a critical regulator of plasma thrombin generation and venous thrombosis. Blood 2008;112(8):3234–3241.

17. Verhenne S, McCluskey G, Maynadié H, et al. Fitusiran reduces bleeding in factor X-deficient mice. Blood 2024;144(2):227–236.

18. Paul DS, Casari C, Wu C, et al. Deletion of the Arp2/3 complex in megakaryocytes leads to microthrombocytopenia in mice. Blood Adv 2017;1(18):1398–1408.

19. Casari C, Paul DS, Susen S, et al. Protein kinase C signaling dysfunction in von Willebrand disease (p.V1316M) type 2B platelets. Blood Adv 2018;2(12):1417–1428.

20. Fressinaud E, Baruch D, Rothschild C, Baumgartner HR, Meyer D. Platelet von Willebrand factor: evidence for its involvement in platelet adhesion to collagen. Blood 1987;70(4):1214–1217.